11A.4 ENHANCING SIGNAL DETECTION IN DUAL-POLARIZATION WEATHER RADARS BY COMBINING THE COHERENCY BASED DETECTION AND 2D DESPECKLING

Igor R. Ivić[(1)(2)], and Valery M. Melnikov[(1)(2)]
(1) Cooperative Institute for Mesoscale Meteorological Studies (CIMMS), The University of Oklahoma
(2) NOAA/OAR National Severe Storms Laboratory, Norman, Oklahoma

1. INTRODUCTION

Proper censoring of the weather radar data on the National Weather Surveillance Radar – 1988 Doppler (i.e., WSR-88D) is essential for the forecasters and automated algorithms. Presently, spectral moments at each range location are censored (i.e., labeled not useful) if the Signal-to-Noise Ratio (SNR) is insufficient, or the echoes from the subsequent trips are overlaid. Current censoring uses power measurements to determine if the SNR is above predetermined threshold relative to the noise power (e.g., 2 dB for reflectivity, and 3.5 dB for velocity measurements). As part of the NPI (NEXRAD Product Improvement) the network of WSR-88D weather surveillance radars (i.e., NEXRAD) is expected to be upgraded to include polarimetric capability. This is to be achieved via a simultaneous transmit and receive of the horizontally and vertically polarized waves; thus, effectively sharing the available power from the transmitter between the two channels. Consequently, the power of the returned echoes in each channel is twice less than in the single-polarization system, resulting in, at least, 3 dB lower SNR. Clearly, if the same censoring scheme is retained, more data will fall below display and processing thresholds and hence will be lost. The actual impact, on operational WSR-88D products and algorithms, using the legacy censoring scheme, was evaluated by Scharfenberg et al. (2005). They have shown that the 3 dB SNR loss leads to an average drop of 5.5%, in detection of weather features, and increases to 8.4% in case of "clear-air" events. Most of the loss occurs in the areas of low reflectivity such as near the tops of convection and along the edges of a weather system. Additionally, the SNR reduction inevitably leads to increase in the errors of estimates. Coupled with the loss in sensitivity, this may impact the velocity-related algorithms and cause the slight increase in the dealiasing errors (especially in the high-shear case), as reported by Scharfenberg et al. (2005). Furthermore, in the recent study by Ice et al. (2011) the average sensitivity loss, caused by the dual polarization modification hardware in the NEXRAD network, was assessed to be 3.5 dB. It is quite clear that the SNR loss has significant impact on the data and it becomes imperative to find the alternative censoring algorithm which would mitigate these adverse effects.

So far, two promising techniques have been proposed. The first one, by Ivić et al. (2009), takes advantage of the signal coherency in sample-time and between the orthogonally polarized returns from the two channels. It is appropriately named the Coherency Based Thresholding (CBT). This technique has been chosen for implementation in the NEXRAD dual-polarization software. A different approach to enhance signal detection has been suggested by Melnikov and Schlatter (2011). It is based on Processing of Noise Speckles (PNS) in two dimensions.

Corresponding author address: Igor R. Ivić, CIMMS/NSSL, 120 David L. Boren Blvd., Norman, OK 73072; email: Igor.Ivic@noaa.gov

2. DESCRIPTION OF METHODS

A censoring approach, that operates on time-series, essentially consists of comparing the output of some function $f(V_h(0,\tau_s),\ldots, V_h(M\text{-}1,\tau_s), V_v(0,\tau_s),\ldots, V_v(M\text{-}1,\tau_s))$ against a threshold to decide if signal is present at a range location τ_s. Complex random variables $V_h(m,\tau_s)$, and $V_v(m,\tau_s)$ are obtained by sampling voltage echoes in horizontal and vertical channels, respectively. The total number of transmissions per dwell is M. In case of the simple SNR censoring, a signal is detected when

$$f=\frac{\frac{1}{M}\sum_{m=0}^{M-1}\left|V_h(m,\tau_S)\right|-N_h}{N_h}\geq THR\ , \tag{1}$$

where N_h is the noise power in the horizontal channel, and THR is the threshold. The expression (1) shows that only increase in power is used as evidence of signal presence. Clearly, SNR based censoring does not make use of the weather signal coherency in sample-time and between channels. Ivić et al. (2009) approach does so by incorporating measurements of autocorrelation and cross-correlation (i.e., correlation between channels) as

$$\begin{aligned} f=&\frac{1}{M}\sum_{m=0}^{M-1}\left(\left|V_h(m)\right|^2+\left|V_v(m)\right|^2\right)+\\ &\frac{1}{M-1}\left|\sum_{m=0}^{M-2}\left(V_h^*(m)V_h(m+1)+V_v^*(m)V_v(m+1)\right)\right| \\ &+\frac{1}{M}\left|\sum_{m=0}^{M-1}V_h^*(m)V_v(m)\right|\geq THR. \end{aligned} \tag{2}$$

The technique by Melnikov and Schlatter (2011) operates on two dimensional censor maps where each location, in the map, is classified as either containing signal or not. Thus, it requires that the time-series are first processed by a censoring scheme that operates on $V_h(m,\tau_s)$ and $V_v(m,\tau_s)$. Such scheme produces a censor map that the PNS can operate on. The simplest approach is applied whereas a signal presence in a shaded bin, at location (n,n) in the map, is considered false if there are no adjacent detections (i.e., it is the sole detection within the boundaries given in Figure 1). Hence, the PNS approach is based on assumption that the probability of detections in adjacent bins is much less when only noise is present and increases with presence of signals. Similar approach, but with extended functionality, is also used by Sigmet 2D 3x3 Speckle Filter (2008).

Let $A(n,n)$ denote the detection event at location, or bin, (n,n) in case when only noise is present. Then, the probability of a false alarm (*PFA*) is

$$\begin{aligned} PFA = P\big(&A(n-1,n-1) \cup A(n-1,n) \cup \\ &A(n-1,n+1) \cup A(n,n-1) \cup A(n,n+1) \cup \\ &A(n+1,n-1) \cup A(n+1,n) \cup A(n+1,n+1) \\ &\big| A(n,n)\big) * P\big(A(n,n)\big), \end{aligned} \tag{3}$$

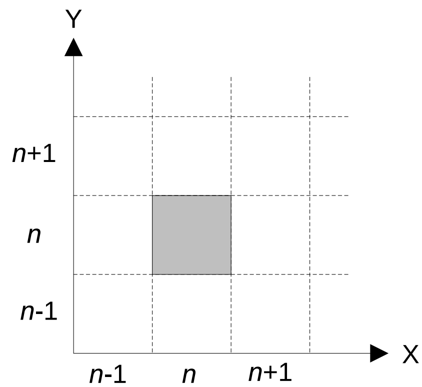

Figure 1. Graphic representation of PNS.

where $\cup$ denotes the *union* of events. The expression (3) can also be written as

$$\begin{aligned} PFA = 1 - P\big(\bar{A}(n,n)\big) - P\big(&\bar{A}(n-1,n-1) \cap \\ &\bar{A}(n-1,n) \cap \bar{A}(n-1,n+1) \cap A(n,n-1) \cap \\ &A(n,n+1) \cap A(n+1,n-1) \cap A(n+1,n) \cap \\ &A(n+1,n+1) \big| A(n,n)\big) * P\big(A(n,n)\big), \end{aligned} \tag{4}$$

where Ā denotes the complementary event of A and $\cap$ stands for *intersection*. If only noise is present and samples used for detection at each location are distinct, we can safely assume that all events are independent. Then we have

$$\begin{aligned} PFA = 1 - &\big(1 - P\big(A(n,n)\big)\big) - \\ &\big[1 - P\big(A(n,n)\big)\big]^8 * P\big(A(n,n)\big). \end{aligned} \tag{5}$$

The expression (5) allows us to compute the rate of false alarms after the PNS is applied, given the PFA at each separate bin. Clearly, any method can be used to generate a censor map. (e.g., SNR or CBT based). To put this into perspective of real applications, let us consider the false alarm rate of $P(A(n,n))=1.17\times10^{-6}$. This PFA is obtained when the number of samples per dwell (M) is 17 and the SNR based censoring is used with the threshold set to 2 dB above the noise level. This is typical of the first scan in the Volume Coverage Pattern 11 (VCP11) in the NEXRAD network. In case of KOUN (WSR-88D research radar located in Norman, OK), the time between subsequent pulse transmissions (i.e., Pulse Repetition Time or PRT) for this scan is 3.1 ms. This translates to 1836 range positions at each dwell; thus, 1836×360 equals 660960 total detection locations in one scan. Given the PFA of 1.17×10^{-6}, and the accurate noise power measurements, we obtain less than a single false detection per scan ($660960\times1.17\times10^{-6} = 0.77$), on the average. If we maintain the current "legacy" censoring on a bin level and apply PNS afterwards, (5) shows the resulting PFA to be 1.1×10^{-11}. Cleary, the use of PNS allows us to relax censoring thresholds when creating a censor map and still retain the same overall PFA, after the PNS application. By solving (5) for the PFA of 1.17×10^{-6}, we get the $P(A(n,n))$ to be 3.8×10^{-4}. Following the formula A8 in Ivić et al. (2009) it can be calculated that, when M is 17, lowering the SNR threshold to 0.1 dB (relative to the noise power), maintains the same overall false alarm rate, in conjunction with the PNS application. By the same rationale, when M is 28 (corresponds to the first scan in VCP21) the SNR threshold of 2 dB yields PFA of 8.64×10^{-10}; hence, we can safely lower this threshold to 0.63 dB and apply "legacy" censoring to obtain the PFA of 1.19×10^{-6}. This however, will still not regain the full 3.5 dB in sensitivity, lost due to the dual-polarization upgrade. We can further lower the SNR threshold to -1.18 dB which results in PFA of 3.77×10^{-4} on a bin level. After processing by PNS, the resulting false detection rate is 1.13×10^{-6}.

Logically, just as the SNR threshold can be relaxed by adding the PNS as the second level of censoring, the same can be done with the CBT. Given the same false alarm rate, the CBT yields improved detection rates compared to the SNR based censoring. Therefore, it is logical to assume that the CBT+PNS combination ought to result in more detections than the SNR+PNS one. This will be investigated further in the text.

3. EVALUATIONS THROUGH SIMULATION

To quantify the improvement, the probabilities of signal detection (PODs) are examined for varied SNR, spectrum widths (σ_v), and differential reflectivites (Z_{DR}) as well as the varied number of signals present in the bins surrounding the central (i.e., shaded) bin in the area shown in Figure 1. Monte Carlo simulations were used (Zrnić 1975) and the detection thresholds were chosen so that the PFA is 1.17×10^{-6}. The ratio of noise powers in vertical (V) and horizontal (H) channels (i.e., N_v/N_h) is set to 0.9. Note that because CBT uses time-series from both channels this ratio influences the detection performance. Figure 2 shows the resulting PODs for varied number of present signals in the bins adjacent to the location (n,n). Because weak signals are primarily of interest, the SNR in horizontal channel is chosen to be 0.5 dB. This is half way between -1 and 2 dB which is the range occupied by signals lost after the 3 dB SNR drop. Also, Z_{DR} is set to 0 dB assuming that, for weak signals, dual-polarization products are not reliable when the vertical channel signal is significantly weaker than the horizontal one. Also, fringes of radar echoes with very low SNR normally contain small droplets with $Z_{DR} \approx 0$ dB or ice crystals with differential reflectivity in the interval 0.5 to 2 dB (Melnikov and Schlatter 2011). The PODs in Figure 2 are calculated as

$$POD_k = 1 - \left[\left(1 - 3.8 \times 10^{-4}\right)^{8-k} \left(1 - POD_S\right)^k POD_S + 1 - POD_S \right], \tag{6}$$

where POD_S is the signal detection probability on a bin level, and is estimated using Monte Carlo simulations. The k stands for the number of signals surrounding the central location. Figure 2 shows that the detection rate significantly declines when k falls below 4 in case of SNR+PNS. For CBT+PNS the same happens for k less than 2. Figure 2 also shows that the CBT+PNS outperforms the SNR+PNS for σ_V of 1 and 3 m s^{-1}.

In Figure 3 the spectrum width dependence is further investigated for k of 8. It also includes the performances for the CBT approach and the single-polarization emulation. The single-polarization PODs are simulated by boosting the SNR by 3 dB and using the "legacy" SNR censoring with the 2 dB threshold. The plot shows that, for the given signal parameters, using solely CBT produces more detections than the SNR+PNS and even surpasses the detection rate of the "legacy" single-polarization model for signals with σ_V up to 2.5 m s^{-1}. As expected, the best detection rate is produced by the CBT+PNS.

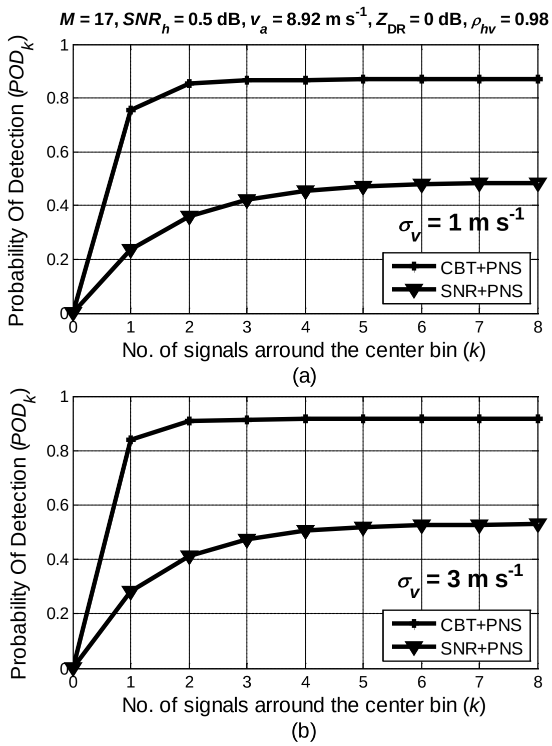

Figure 2. PODs for varied number of present signals in the bins surrounding the central location for (a) σ_V = 1 m s^{-1}, and (b) σ_V = 3 m s^{-1}.

Figure 4 and Figure 5 present PODs for a range of SNR and Z_{DR} values. In both cases σ_V is set to 2 m s^{-1} because Fang et al. (2004) established that it is the median value for most weather events of interest. As expected, POD is directly proportional to the SNR regardless of the censoring approach. Naturally, differential reflectivity has no impact on the SNR based censoring. When CBT is used, the POD is inversely proportional to Z_{DR}. Compared to the SNR+PNS, the CBT+PNS performs better for all simulated parameters.

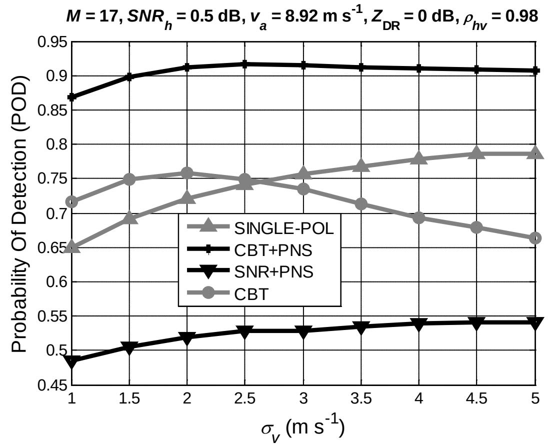

Figure 3. PODs for varied spectrum widths.

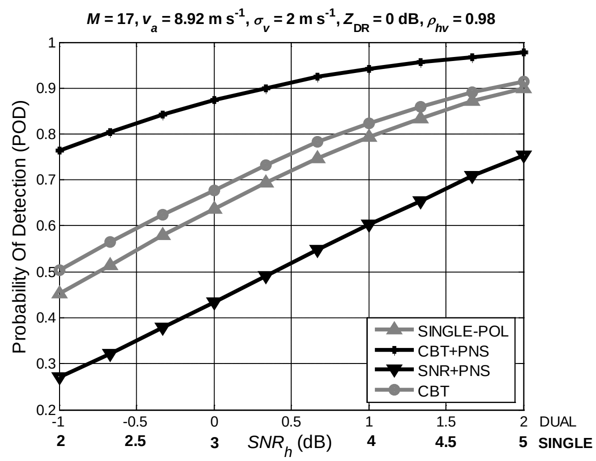

Figure 4. PODs for a range of SNR.

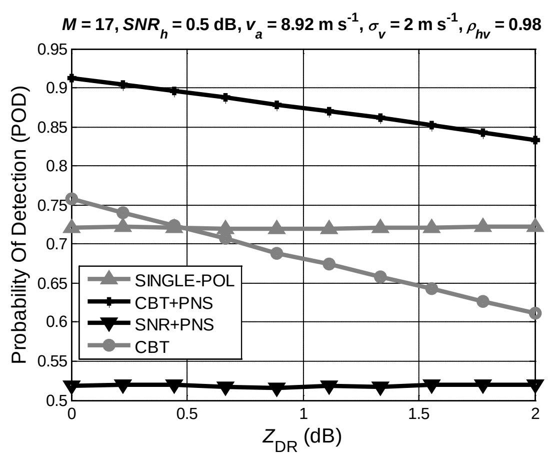

Figure 5. PODs for a range of Z_{DR} values.

Next, the same analysis is carried out for M of 28. Again, the CBT threshold was adjusted to produce PFA of 3.8×10^{-4} and the SNR one is lowered even further to -1.18 dB resulting in 3.77×10^{-4} PFA on a bin level; thus, yielding overall 1.13×10^{-6} false detection rate after the PNS. Figure 6 shows that, as the number of samples had increased, the POD improved. Also, it became less sensitive to the number of signals present in surrounding bins. In this particular case, the POD decreases significantly only when the number of bins containing signal fall below 1 for CBT+PNS, and 3 for SNR+PNS.

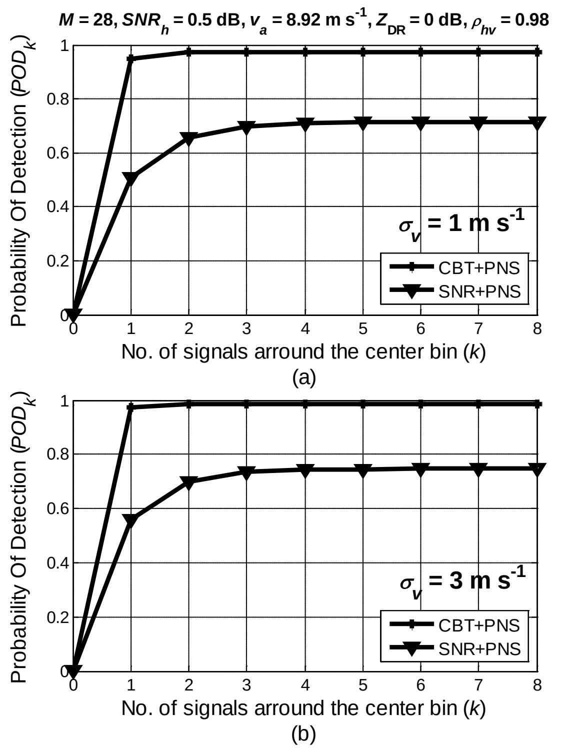

Figure 6. PODs for varied number of present signals in the bins surrounding the central location for (a) σ_v = 1 m s^{-1}, and (b) σ_v = 3 m s^{-1}.

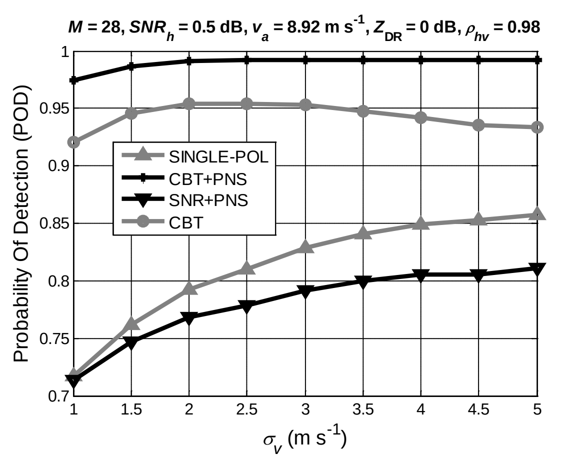

Figure 7. PODs for varied spectrum widths.

Figure 7 shows that while the SNR+PNS POD approaches that of the single-polarization, it is still unable to produce full recovery from the 3 dB SNR drop. On the other hand, CBT and CBT+PNS not only regain the full sensitivity but even increase it, in this case. Figure 8 gives further evidence that, for coherent signals, despite the loss in signal strength, the CBT+PNS produces increase in sensitivity, compared to legacy single-polarization SNR censoring. Investigation into the differential reflectivity dependence is presented in Figure 9. It gives evidence of sensitivity improvement produced by CBT+PNS. Comparison between CBT and CBT+PNS shows the latter to be less sensitive to Z_{DR} drop.

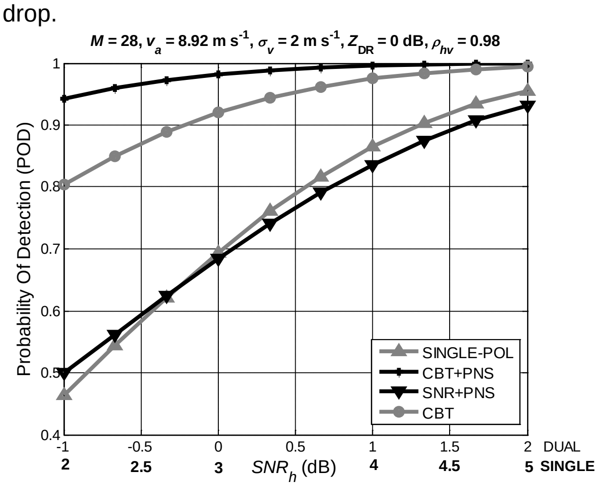

Figure 8. PODs for a range of SNR.

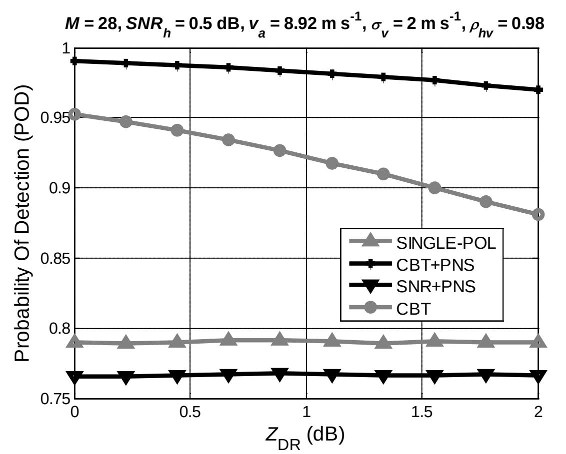

Figure 9. PODs for a range of Z_{DR} values.

So far, simulations have shown that the CBT coupled with the PNS produces more signal detections compared to other approaches investigated. To further corroborate such results, performance on time-series is presented next.

4. TIME-SERIES IMPLEMENTATION

Real data evaluation is performed using the set of dual-polarization time series. The first set was collected with the dual-polarization WSR-88D Vance (KVNX) radar, at a PRT of 3.1 ms, with M = 17, and at elevation of 0.57 deg while executing the first surveillance scan in the VCP11. This radar operates at a wavelength of

10.355 cm resulting in an unambiguous velocity of 8.33 m s^{-1}. Therefore, this collection corresponds to the first set of simulations with an unambiguous velocity of 8.92 m s^{-1}. Time-series were processed with the standard pulse pair estimators (Doviak and Zrnić 1993), and using radial based noise estimation (Ivić and Torres 2011). No clutter removal has been applied. Because the main objective of increasing the radar sensitivity, in case of NEXRAD network, is retrieval of the lost signals due to the SNR drop, the proposed techniques are applied only to data bins with the SNR smaller than the legacy threshold. For this particular data set, these "weak signals" have power less than 2 dB, with respect to noise. All other data bins with SNR larger than the legacy threshold are considered valid detections that require no further censoring (e.g., PNS). The total number of detections produced by SNR+PNS is 125614. Out of these, 9635 (7.7%) were weak signals (i.e., SNR less than 2 dB). When solely CBT was used, it produced 132867 detections, where 16888 (12.7%) were weak. Application of CBT+PNS resulted in 141484 detections, out of which 25505 (18%) were weak. Ratios with respect to SNR+PNS are given in Table 1. Note that the CBT+PNS produces 12.6% more coverage, and 2.65 times increase in weak detections than the SNR+PNS; hence, these numbers support the results obtained by simulations. Let us analyze the features of weak signal detections. There are 16271 locations where weak signal detections occurred when CBT+PNS was used but were missed by the SNR+PNS. Figure 10 (a) shows the distribution of the magnitude of the normalized autocorrelation estimate at lag 1 (i.e., autocorrelation coefficient) vs. correlation coefficient magnitude (Doviak and Zrnić 1993) estimate for these detections. It suggests that the majority of detections lie in the area of high coherency either along sample-time or between channels, or both. Hence, detections which have weak coherency in sample-time exhibit significant coherency between channels and vice versa. This is logical because the CBT relies on signal coherencies to improve detection. Important aspect when dealing with weak signals is the quality (i.e., accuracy) of estimates. For instance, if the SNR in H channel is used for censoring, the power estimate in V channel can be less than the noise when signal is weak. Consequently, it puts in question the accuracy of polarimetric estimates, at the corresponding location, even if lag 1 estimators are used (Melnikov and Zrnić 2004); thus, rendering such detection unusable for polarimetric measurements. Naturally, this is not the problem when CBT is used for censoring, because it utilizes power estimates from both channels. Nonetheless, as estimates are obtained from low SNR signals, the variances of estimates are large which means that the measurements of the correlation coefficient magnitude can easily have values larger than unity; thus, making the estimates physically unfeasible. In this particular case, 47% out of the additional 16271 detections have correlation coefficient estimate less than one, when lag 1 estimator is used, as opposed to 35% in case of standard estimator (i.e., the one using signal power estimates from both channels and the magnitude of the cross channel correlation). This seems logical because the lag 1 estimator is less sensitive to noise and most weak CBT+PNS detections exhibit strong autocorrelation coefficients which favors the lag 1 estimator. Additionally, there are 401 weak detections that are picked up by the SNR+PNS but are missed by the CBT+PNS. Out of those, however, only 204 (or 50.9%) have vertical channel power larger than the noise and are usable for polarimetric variable computations. When it comes to correlation coefficient, it becomes interesting that 60% of estimates are less than one when standard estimator is used, but this drops to 34% for the lag 1 estimator. Possible explanation is that the SNR+PNS favors detections less coherent in sample-time. Evidence of this is in Figure 10 (b), which shows that the SNR+PNS detections are far more dispersed in terms of the autocorrelation and the correlation coefficient than those from the CBT+PNS. Lower coherency in sample-time results in more accurate power estimates but less accurate autocorrelation measurements. First are used in the standard and the latter in the lag 1 estimator. Consequently, the standard estimator performs better than the lag 1 for less coherent detections. On the contrary, in case of CBT+PNS, we have reversed situation which results in more accurate, in general, estimates produced by the lag 1 estimator. As evidence of this, we have seen that, for the CBT+PNS additional detections, more estimates of correlation coefficient fall below unity when lag 1 estimator is used. This is also seen in Table 1 where the ratio of valid correlation coefficient ($|\rho_{hv}(0)|$) estimates declines, compared to the ratio of weak signal detections, when lag 0 (i.e., standard) estimator is used, but increases for lag 1 estimator. Generally, for detections with SNR larger than 2 dB, 84.5% have $|\rho_{hv}(0)|$ less than one when standard estimator is used versus 75% produced by the lag 1 estimator. The histograms of SNR and reflectivity distributions are shown in Figure 11. Number in each histogram bin is scaled by the total number of weak detections produced by the SNR+PNS. It is interesting to notice that, in this case, the large portion of weak detections, for the CBT and the CBT+PNS, goes toward signals with SNR below 0 dB. These are most likely detections that exhibit strong coherency in sample-time or between channels, or both. The SNR+PNS, however, is limited to signals with SNR above 0.1 dB. Visualization of improvements, produced using CBT+PNS, is shown in Figure 12. Additional detections, with respect to the SNR+PNS, are highlighted in white.

D	CBT	CBT+PNS
Ratio of total detections	1.0577	1.12634
Ratio of weak detections (SNR < 2dB)	1.75278	2.647
Ratio of valid V powers (SNR < 2dB)	1.7894	2.7024
Ratio of valid $|\rho_{hv}(0)|$ using standard est. *(SNR < 2dB)*	1.5244	2.199
Ratio of valid $|\rho_{hv}(0)|$ using lag 1 est. *(SNR < 2dB)*	1.8022	2.683

Table 1. Detection statistics with respect to SNR+PNS for the surveillance scan with M = 17.

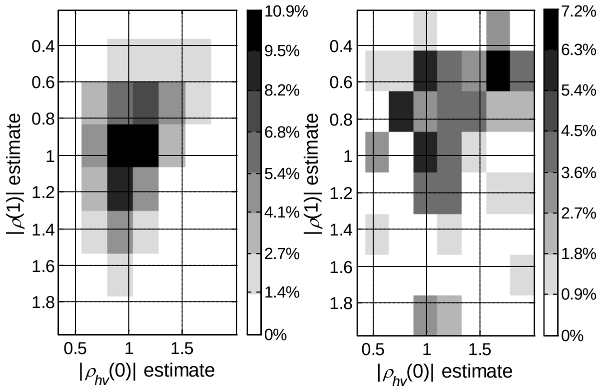

(a) (b)

Figure 10. (a) Distribution of 16271 detections picked by CBT+PNS but missed by SNR+PNS. (b) Distribution of 401 detections picked by SNR+PNS but missed by CBT+PNS. The SNR threshold is 2 dB, and M = 17.

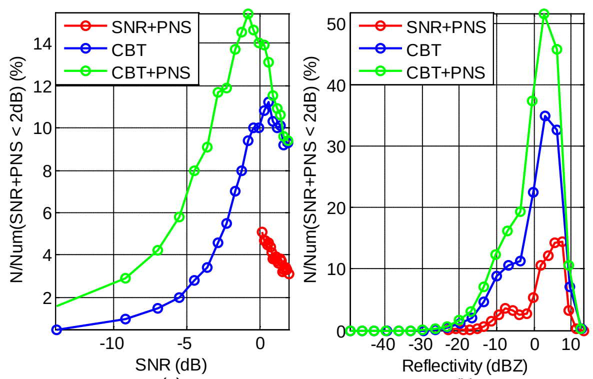

(a) (b)

Figure 11. Histograms of (a) SNR and (b) reflectivity for weak detections (i.e., SNR < 2 dB).

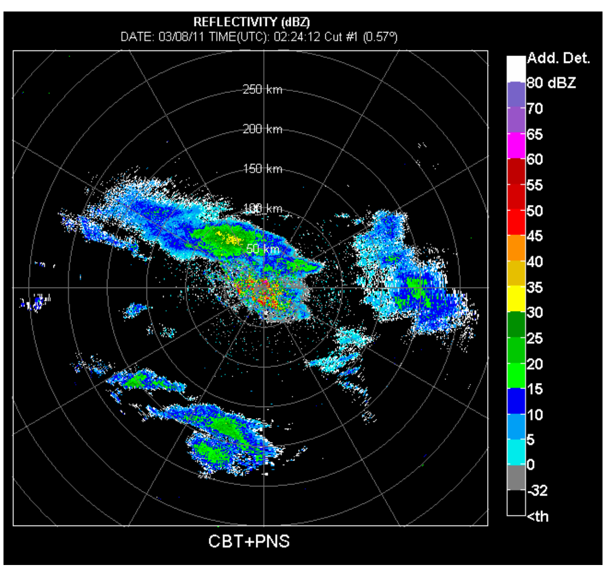

Figure 12. Reflectivity field obtained with CBT+PNS with additional detections, with respect to SNR+PNS, highlighted in white (M = 17).

Further investigation is carried on data from the same collection where the Doppler scan had M of 61 and unambiguous velocity of 30.57 m s^{-1}. This data is combined with that from the surveillance scan which was analyzed previously. Data from the long PRT scan (i.e., surveillance) is used for range unfolding which is a procedure used in weather radars that produces velocity measurements at long ranges with unambiguous velocities that correspond to much shorter range (but larger unambiguous velocity) transmission PRT. Two consecutive scans are performed. The first is with long PRT (i.e., surveillance) which yields long unambiguous range, but modest unambiguous velocity due to the phase folding. The second scan is with the short PRT (i.e., Doppler) which yields larger unambiguous velocity but produces echoes that contain sum returns from several trips (i.e., overlaid echoes). Signal power measurements are obtained from the long PRT in such manner that the noise power is subtracted from the total estimated power. Signal power is set to zero where subtraction yields negative value. So obtained measurements are used to determine ranges at which echoes from several trips are overlaid and whether valid information about Doppler velocity can be extracted from estimates at such range locations (i.e., if echo at such range locations can be resolved). A range location, that contains several overlaid echoes, is deemed resolved only if the power, obtained from the surveillance scan, of one of the overlaid echoes is larger than the sum of the rest by a user-specified value (usually 5 dB), and the echo is not censored. In such case, the velocity estimate, obtained from the Doppler scan, is assigned to the range location having the echo with the largest power. Range locations having weaker power are then flagged as obscured and Doppler data is suppressed at those locations (usually shown as ‘'purple haze” in the velocity field). Because of the PNS processing, detections, in Doppler scan, are produced by lowering the SNR threshold to -3.77 dB. This results in the false alarm rate of $3.8{\times}10^{-4}$. Using the map generated from the surveillance scan data, these detections are classified as resolved, or not, and assigned proper range locations. Note that the same overlaid map is used regardless of the censoring approach in the Doppler scan. Application of PNS produces overall PFA of $1.17{\times}10^{-6}$, and the total number of detections, not counting the “purple haze” (i.e., overlaid echoes), is 98459. Out of these 5064 (5.1%) are “weak” signals with SNR below 3.5 dB, in Doppler scan. Using only CBT, with the threshold set to yield PFA of $1.17{\times}10^{-6}$, in Doppler scan, results in 98956 total, and 5561 (5.6%) weak detections. Finally, just as with the SNR+PNS, CBT+PNS thresholds were lowered to result in the PFA of $3.8{\times}10^{-4}$, and the final censoring is done by the PNS. Consequently, CBT+PNS produced 99059 total, and 5664 (5.7%) weak detections. The resulting velocity field, with additional detections obtained using CBT+PNS is presented in Figure 13, where additional detections with respect to the SNR+PNS are highlighted in white. The statistics is given in Table 2.

Comparison between statistics in Table 1 and Table 2 reveals that the improvement over the SNR+PNS, obtained by the CBT+PNS, is negligible in the split scan.

D	CBT	CBT+PNS
Ratio of total detections	1.00505	1.0061
Ratio of weak detections (SNR<2 dB)	1.098144	1.118483

Table 2. Detection statistics with respect to SNR+PNS for the split scan with *M* equaling 17 and 53 in the surveillance and Doppler scan, respectively.

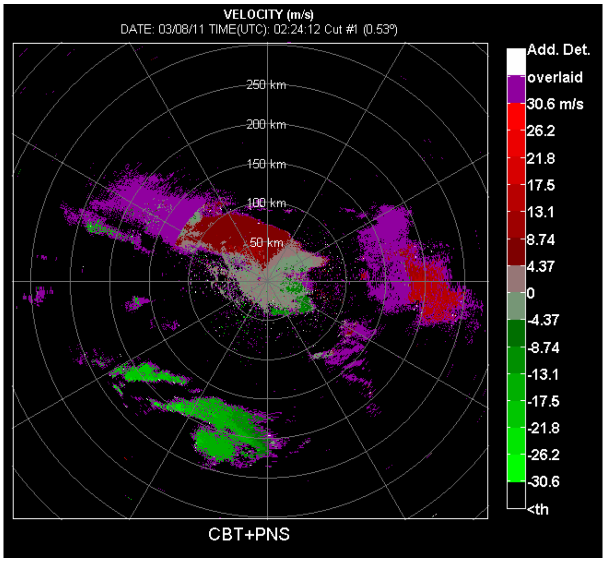

Figure 13. Velocity field obtained after lowering the CBT threshold, in Doppler scan, and applying the PNS (M = 17&61). Additional detections, with respect to the SNR+PNS, are highlighted in white.

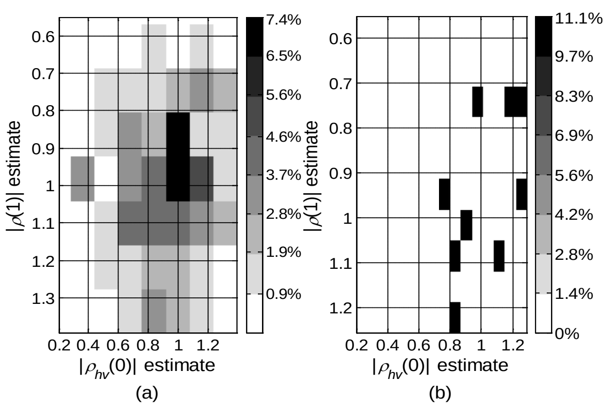

Figure 14. (a) Distribution of 634 detections picked by CBT+PNS, but missed by SNR+PNS. (b) Distribution of 33 detections picked by SNR+PNS, but missed by CBT+PNS. The split scan (M = 17&61).

It shows that the performance of all three approaches is quite similar with the CBT and CBT+PNS producing about 10% improvement in weak detections over the SNR+PNS. However, In view of the total detections this improvement is negligible. Accordingly, visual inspection of Figure 13 reveals no significant number of additional detections that are highlighted in white (as they are picked by the CBT+PNS but not by the SNR+PNS). This is to be expected because there are total of only 632 (0.6%) of those. Figure 14 (a) shows that most of these detections exhibit strong coherencies. At the same time, major differences in Figure 15 become visible after the SNR drops below the SNR+PNS threshold (i.e., -3.77 dB), so much so that a large portion of CBT+PNS weak detections are signals with the SNR so low that it puts in question the validity of corresponding estimates.

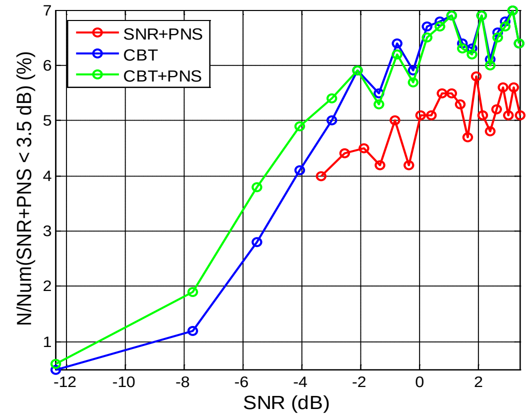

Figure 15. Histogram of SNR for weak detections (i.e., SNR < 3.5 dB).

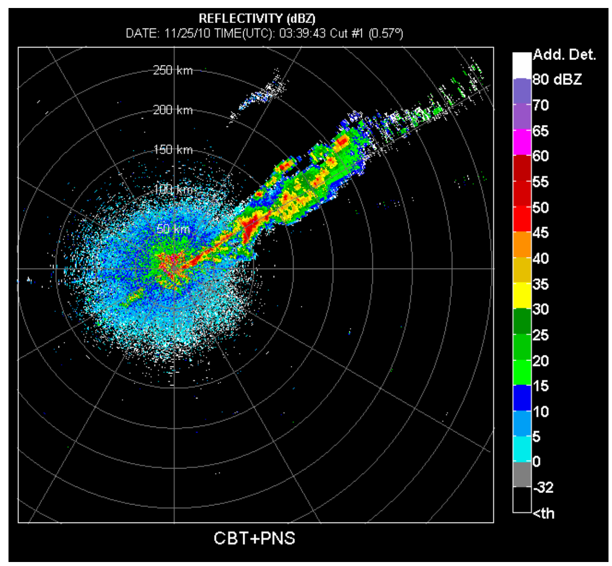

Figure 16. Reflectivity field obtained with the CBT+PNS with additional detections, with respect to the SNR+PNS, highlighted in white (M = 28).

Another, test case is presented next. This set was collected with the dual-polarization research WSR-88D (KOUN) radar, at a PRT of 3.1 ms. The number of samples M is now larger and equals 28, at elevation of 0.57 deg. This corresponds to the second set of simulations with an unambiguous velocity of 8.92 m s^{-1}, which further corresponds to the first scan in VCP21. The total number of detections produced by SNR+PNS is 148666. Out of these, 12276 (8.26%) were weak signals with SNR less than 2 dB. CBT produced 153847 detections, where 17457 (11.35%) were weak signals. Application of CBT+PNS resulted in 159436 detections, out of which 23046 (14.45%) were weak. Ratios with respect to SNR+PNS are given in Table 3. Again, these numbers support the results obtained by simulations. Figure 16 shows the reflectivity field that is obtained with the CBT+PNS, where the additional detections, with respect to the SNR+PNS, are shown in white.

D	CBT	CBT+PNS
Ratio of total detections	1.038	1.0724
Ratio of weak detections (SNR < 2dB)	1.422	1.8773
Ratio of valid V powers (SNR < 2dB)	1.4456	1.9084
Ratio of valid $\lvert\rho_{hv}(0)\rvert$ using standard est. *(SNR < 2dB)*	1.3196	1.695
Ratio of valid $\lvert\rho_{hv}(0)\rvert$ using lag 1 est. *(SNR < 2dB)*	1.4658	1.8896

Table 3. Time-series statistics with respect to SNR+PNS for the surveillance scan with M = 28.

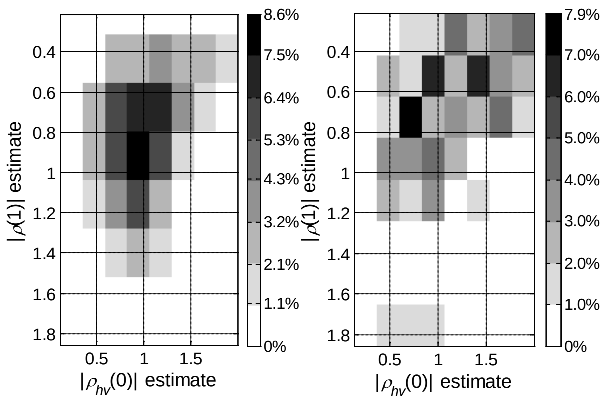

Figure 17. (a) Distribution of 11194 detections picked by the CBT+PNS but missed by the SNR+PNS. (b) Distribution of 424 detections picked by the SNR+PNS but missed by the CBT+PNS. The SNR threshold is 2 dB, and M = 28.

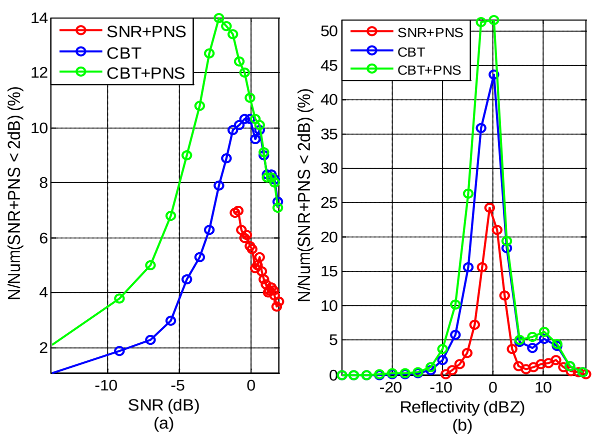

Figure 18. Histograms of (a) SNR and (b) reflectivity for weak detections (i.e., SNR < 2 dB).

There are 11194 detections that are missed by the SNR+PNS but picked by the CBT+PNS, and 424 vice versa. Out of the latter ones, 224 (52.8%) have vertical signal power estimate larger than one, and can produce reliable polarimetric variables. Figure 17 shows the distribution of these detections with respect to the autocorrelation and correlation coefficients. It exhibits the same behavior as in the previous case. The statistics presented in Table 3 further confirms this.

The previous data set obtained during the surveillance scan is combined with the Doppler scan, with M of 90 and unambiguous velocity of 30.8 m s^{-1}. Just like in the previous case, the surveillance scan was used for range unfolding. Due to the high number of samples in the dwell, the SNR threshold was lowered to -4.05 dB, with respect to the noise power. This results in the overall PFA of 1.17×10^{-6} after application of PNS. The combination SNR+PNS obtains the total of 120459 detections, out of which 10036 (8.3%) are weak signals. Use of CBT, for censoring in Doppler scan, produces 121675 detections, and 11252 (9.2%) with SNR below 3.5 dB. As expected, CBT+PNS produces the most detections. The total is 122384, with weak signals being 11961 (9.8%). The statistics is given in Table 4, and the velocity field in Figure 19. The numbers of detections picked by the CBT+PNS, but missed by SNR+PNS, is 1963. Contrary, there are only 38 detections vice versa, and only 11 of those have positive vertical signal power estimate. Distributions are presented in Figure 20 and histograms for weak detections in Figure 21.

D	CBT	CBT+PNS
Ratio of total detections	1.0101	1.01598
Ratio of weak detections (SNR< 2 dB)	1.12116	1.1918

Table 4. Time-series statistics with respect to SNR+PNS, for the split scan with M equaling 28 and 90 in the surveillance and Doppler scan, respectively.

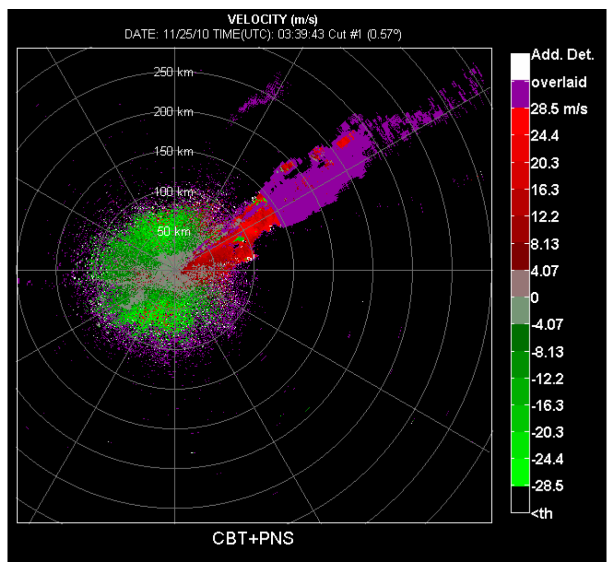

Figure 19. Velocity field obtained after lowering the CBT threshold in Doppler scan and applying the PNS (M = 28&90). Additional detections, with respect to SNR+PNS, are highlighted in white.

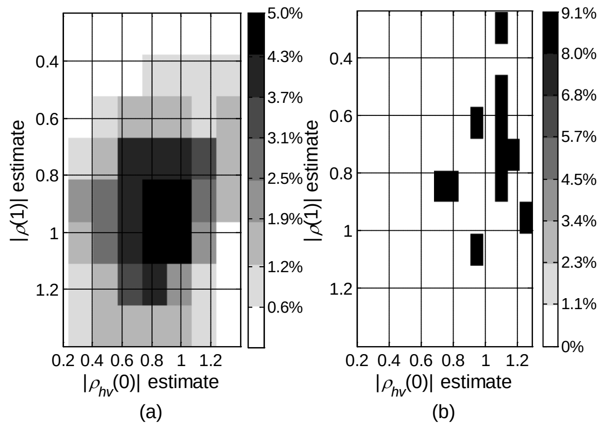

(a) (b)

Figure 20. Distribution of 1963 detections picked by CBT+PNS but missed by SNR+PNS. (b) Distribution of 38 detections picked by SNR+PNS but missed by CBT+PNS. The corresponding split scan (M = 28&90) velocity field is in Figure 19.

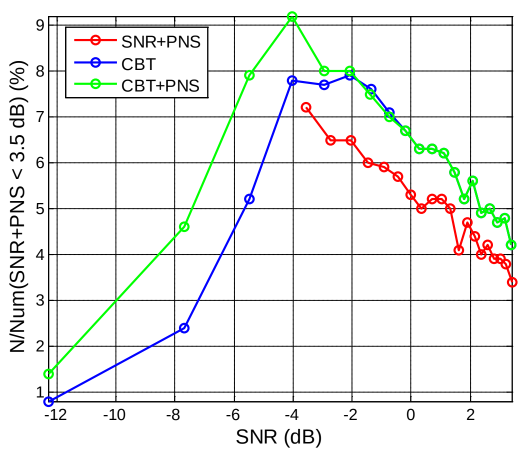

Figure 21. Histogram of SNR for weak detections (i.e., SNR < 3.5 dB). The corresponding data velocity field is in Figure 19.

Three more examples are presented further. In all cases data was collected by the research WSR-88D KOUN radar. By examining individual statistics for each example, one notices that most of the improvement, from using the CBT or CBT+PNS over SNR+PNS, occurs in the surveillance scans, while performances are similar in the split scans. This is corroborated by the averaged statistics in Table 8.

D	CBT	CBT+PNS
Ratio of total detections	1.0655	1.1545
Ratio of weak detections (SNR < 2dB)	1.648	2.528
Ratio of valid V powers (SNR < 2dB)	1.681	2.578
Ratio of valid |ρ_{hv}(0)| using standard est. *(SNR < 2dB)*	1.439	2.116
Ratio of valid |ρ_{hv}(0)| using lag 1 est. *(SNR < 2dB)*	1.66	2.476

(a)

D	CBT	CBT+PNS
Ratio of total detections	1.0127	1.0158
Ratio of weak detections (SNR< 2 dB)	1.1153	1.1437

(b)

Table 5. Time-series statistics with respect to SNR+PNS (a) for the surveillance scan in Figure 22, and (b) the split scan in Figure 22.

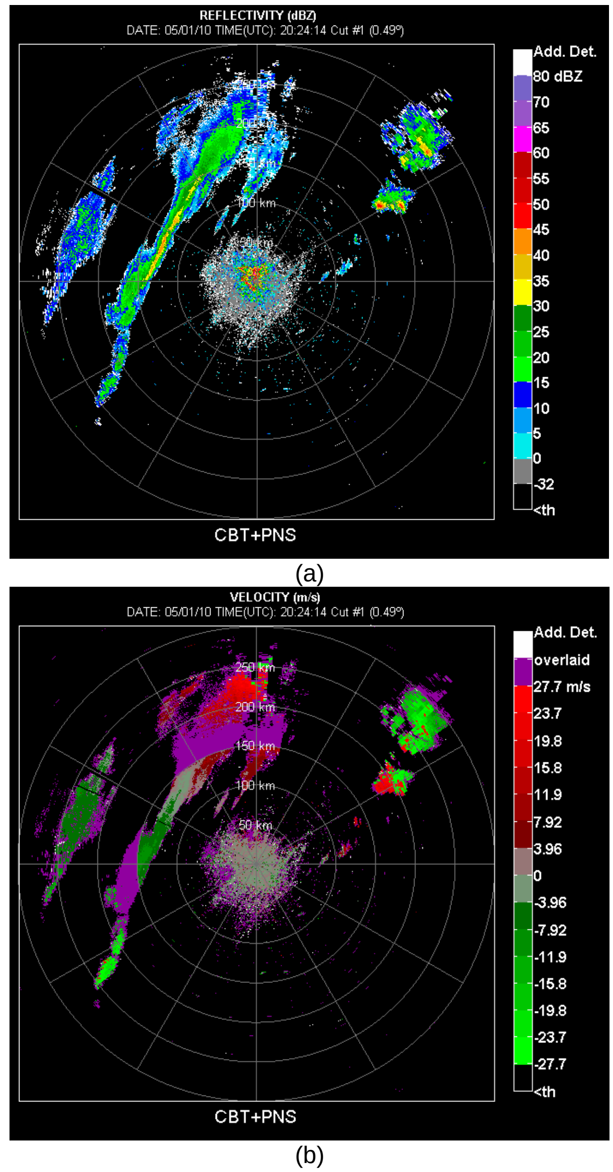

(a) (b)

Figure 22. (a) Reflectivity (M = 17), and (b) velocity (M = 17&52) field obtained with CBT+PNS with additional detections, with respect to SNR+PNS, highlighted in white.

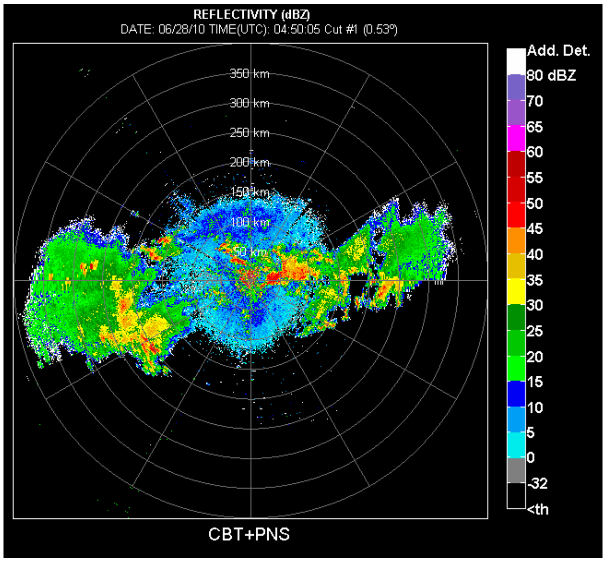

(a)

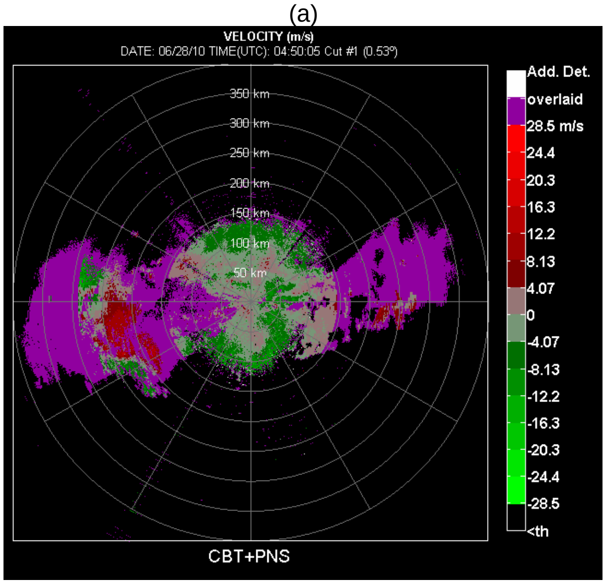

(b)

Figure 23. (a) Reflectivity (M = 17), and (b) velocity (M = 17&53) field obtained with CBT+PNS with additional detections, with respect to SNR+PNS, highlighted in white.

D	CBT	CBT+PNS
Ratio of total detections	1.0012	1.03127
Ratio of weak detections (SNR< 2 dB)	1.0276	1.704
Ratio of valid V powers (SNR < 2dB)	1.4456	1.9084
Ratio of valid $\lvert\rho_{hv}(0)\rvert$ using standard est. *(SNR < 2dB)*	0.8154	1.3834
Ratio of valid $\lvert\rho_{hv}(0)\rvert$ using lag 1 est. *(SNR < 2dB)*	0.965	1.5846

(a)

D	CBT	CBT+PNS
Ratio of total detections	1.0001	1.0008
Ratio of weak detections (SNR< 2 dB)	1.00312	1.02337

(b)

Table 6. Time-series statistics with respect to SNR+PNS (a) for the surveillance scan in Figure 24, and (b) the split scan in Figure 24.

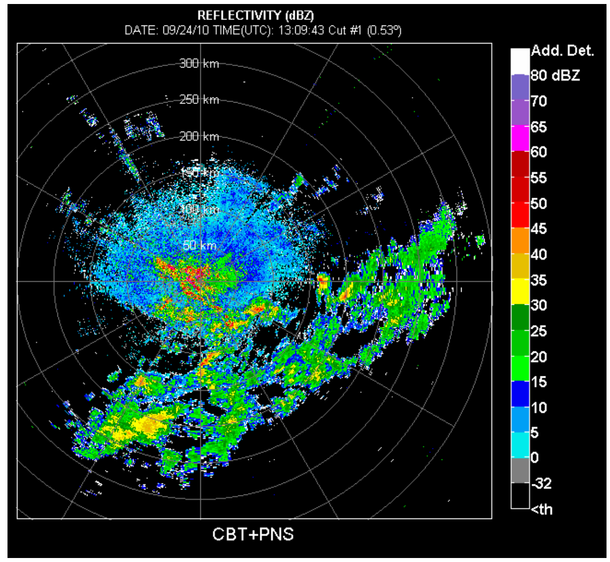

(a)

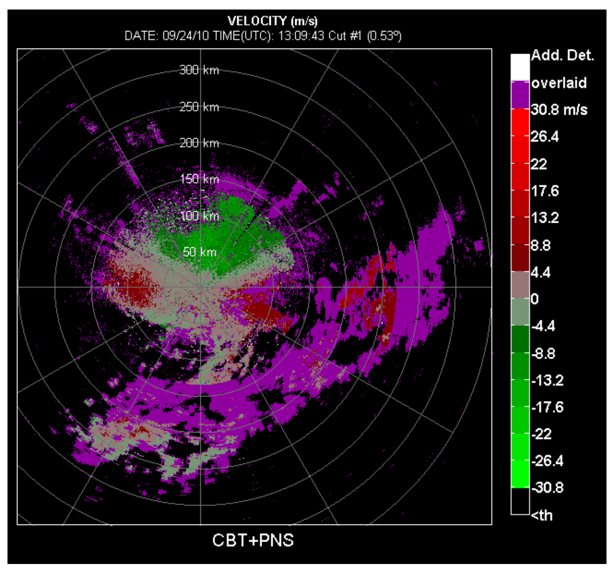

(b)

Figure 24. (a) Reflectivity (M = 28), and (b) velocity (M = 28&97) field obtained with CBT+PNS with additional detections, with respect to SNR+PNS, highlighted in white.

D	CBT	CBT+PNS
Ratio of total detections	1.0004	1.04165
Ratio of weak detections (SNR< 2 dB)	1.0042	1.4378
Ratio of valid V powers (SNR < 2dB)	1.0982	1.5723
Ratio of valid $\lvert\rho_{hv}(0)\rvert$ using standard est. *(SNR < 2dB)*	0.8496	1.195
Ratio of valid $\lvert\rho_{hv}(0)\rvert$ using lag 1 est. *(SNR < 2dB)*	0.93287	1.325

(a)

D	CBT	CBT+PNS
Ratio of total detections	1.001	1.0019
Ratio of weak detections (SNR< 2 dB)	1.019	1.0363

(b)

Table 7. Time-series statistics with respect to SNR+PNS (a) for the surveillance scan in Figure 24, and (b) the split scan in Figure 24.

D	CBT	CBT+PNS
Ratio of total detections	1.03257	1.085232
Ratio of weak detections (SNR< 2 dB)	1.3709	2.03882
Ratio of valid V powers (SNR < 2dB)	1.49195	2.1339
Ratio of valid $\lvert\rho_{hv}(0)\rvert$ using standard est. *(SNR < 2dB)*	1.1896	1.71768
Ratio of valid $\lvert\rho_{hv}(0)\rvert$ using lag 1 est. *(SNR < 2dB)*	1.3652	1.99164

(a)

D	CBT	CBT+PNS
Ratio of total detections	1.006	1.008
Ratio of weak detections (SNR< 2 dB)	1.0713	1.103

(b)

Table 8. Averaged statistics with respect to SNR+PNS (a) for the surveillance scan, and (b) the split scan.

It certainly comes across as interesting that differences in performance are minimal in the split scans. This, however, is not so much a surprise if we take a note of the fact that the map of overlaid echoes is created based on the power difference criteria and is, thus, the same for all detection approaches. Therefore, the only difference is in Doppler scan detections. This difference is further diminished because only detections that are resolved are taken as valid.

5. ASSESSMENT OF DATA RECOVERY

To assess the degree to which the SNR+PNS and CBT+PNS recover detections, lost after the SNR drop, the noise power is artificially increased in each data set presented so far. In particular, because mitigation of sensitivity loss, due to the dual polarization hardware in WSR-88D, is of interest, an assessment of 3.5 dB by Ice et al. was used to artificially increase noise. To give reader an idea of the impact the SNR decrease imparts on censoring, the reflectivity field, with lost detections highlighted in white, is shown for each data set. It is followed by the classification of detections for SNR+PNS, CBT, and CBT+PNS. Each example is concluded by the table summarizing the statistics. The first column, marked as SNR, presents information obtained after artificially increasing noise and applying the SNR threshold of 2 dB, in surveillance, and 3.5 dB in Doppler scan. It gives statistical assessment of the SNR drop impact. The same is given for SNR+PNS, CBT, and CBT+PNS. The row denoted as 'Lost' gives the amount of data lost with respect to the legacy censoring with the SNR higher by 3.5 dB (i.e., no noise increase). Percentages of detections that are the same, before and after noise amplification, are shown in the row below. Information for data that is originally censored by the legacy thresholding, but is classified as signals after noise increase, is presented in the row labeled as 'Additional'. Note that the SNR censoring, produces minimal number of additional detections. This can be viewed as the artifact of statistical processing. Namely, the noise power, measured using Ivić and Torres (2011), is used as basis to simulate noise samples using the pseudorandom number generator. These are then added to the data. Consequently, some of the powers, which were below threshold, before noise addition, exceed the threshold afterwards. The last row shows the percentages of recovered signals, with SNR between the legacy threshold value and the one 3.5 dB higher. These are the signals which are lost due to the SNR drop, so these percentages provide good assessment of the recovery effectiveness produced by each technique. Finally, average statistic, for surveillance and split scan, is given in Table 19.

Visual examination reveals significant loss of coverage, caused by the SNR decrease, both in the reflectivity and velocity fields. The averaged statistics associates numbers to this loss. These are 13%, and 10.8% for reflectivity and velocity fields. In surveillance scan, the SNR+PNS produces the poorest performance on the average. It recovers bit more than 94% of the lost data (60.7% for data with SNR less than 5.5 dB) and detects 1.3% additional. CBT fares a bit better by recovering 96% (70.5% with SNR<5.5 dB) and producing 3% additional detections. Altogether, CBT yields 99% detections which implies that, in the sum, CBT almost regains the coverage of the legacy system. CBT+PNS recovers 98% (85% for SNR<5.5 dB) and adds 6.3% of additional data; thus, producing coverage which is 104% of that in the legacy system. Clearly, CBT+PNS not only yields the highest signal recovery but produces noticeably more coverage than the legacy censoring with the SNR 3.5 dB higher. Consequently, this can be very significant in a field of weak echoes which is more susceptible to the drop in SNR. Contrary to the surveillance, in the split scan, the average overall recovery is about 97% for all three techniques. The most likely reason for the similar performance of all techniques is that the same overlaid map is used for all techniques. Consequently, the only difference is in detections gained during Doppler scan. This difference is further diminished because unresolved detections, from Doppler scan, are discarded; thus leading to practically same performances for all techniques.

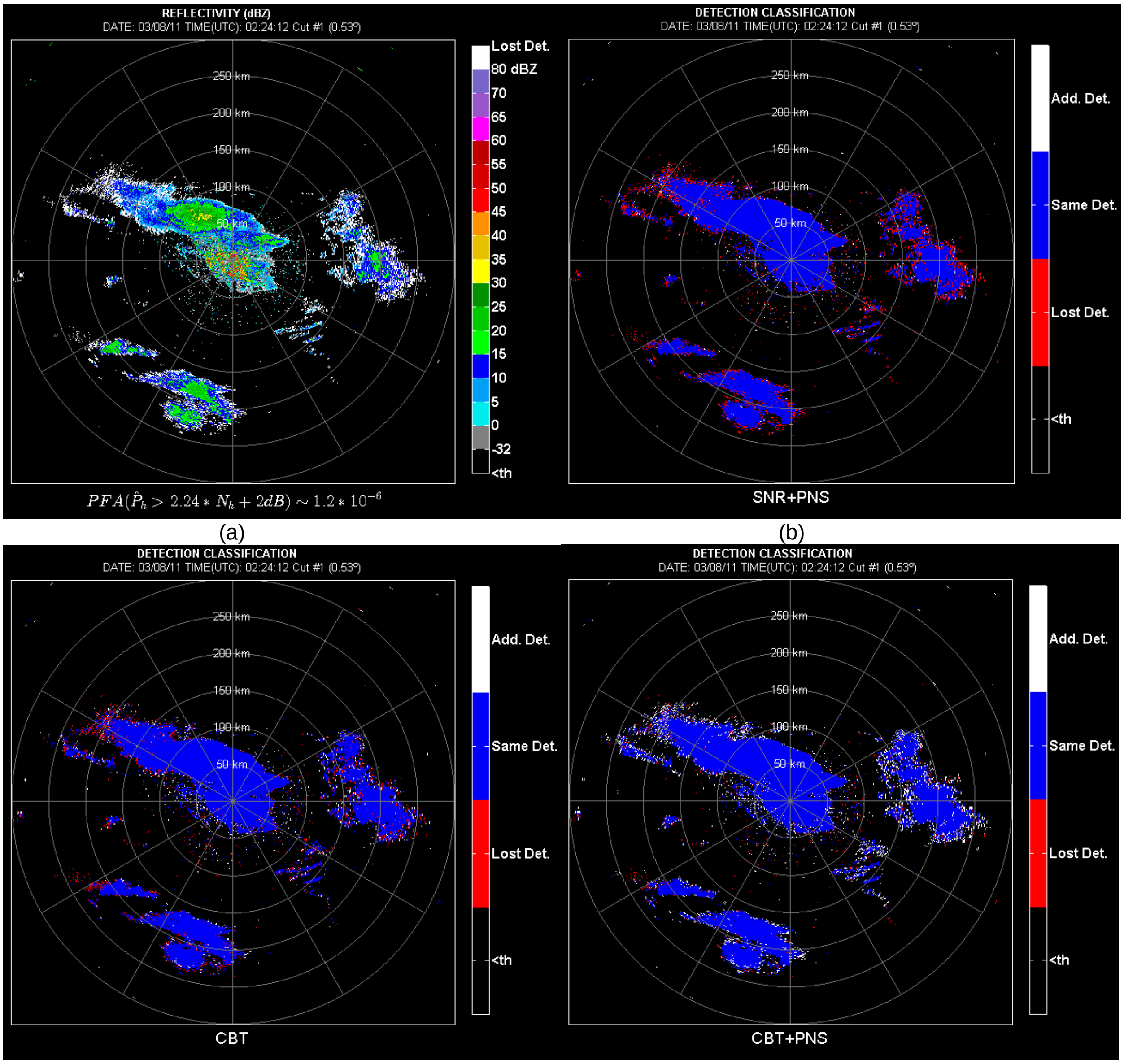

Figure 25. (a) Reflectivity field (M = 17) obtained after artificially increasing the noise power and setting the SNR threshold to 2 dB with respect to the increased noise power. The lost detections are highlighted in white. Classification of detections for (b) SNR+PNS, (c) CBT, and (d) CBT+PNS.

Detections (%)	SNR	SNR+PNS	CBT	CBT+PNS
Lost	14.2	7.7	4.3	2
Same	85.8	92.3	95.7	98
Additional	0.6	1.2	3.2	7.2
Total	86.4	93.5	98.9	105.2
Recovered signals with SNR < 5.5 dB	12.5	48	71	86.6

Table 9. Comparison statistics with respect to the SNR censoring with the original noise power.

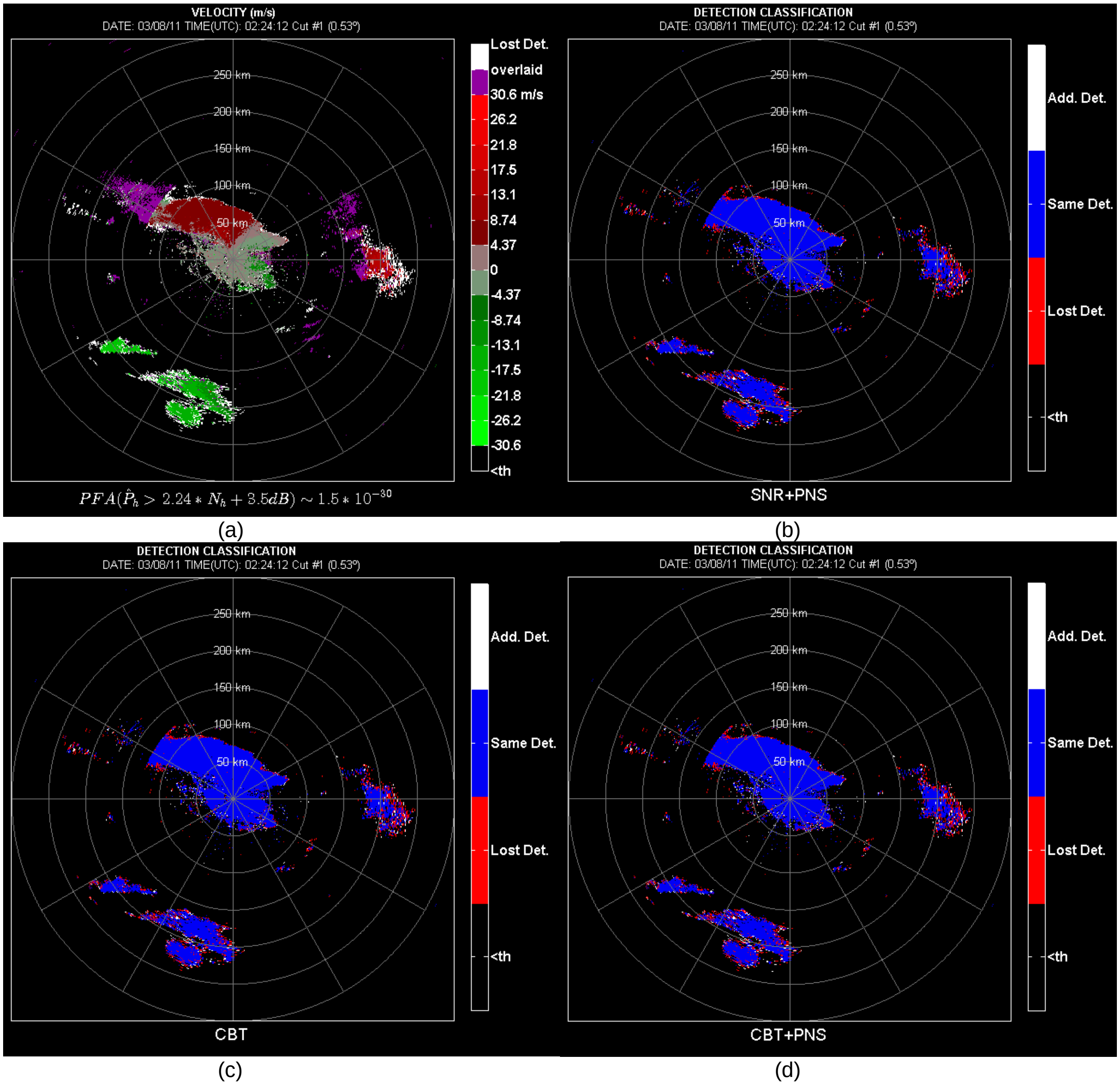

Figure 26. (a) Velocity field (*M* = 17&61) obtained after artificially increasing the noise power and setting the SNR threshold to 2 dB with respect to the increased noise power. The lost detections are highlighted in white. Detection classification for (b) SNR+PNS, (c) CBT, and (d) CBT+PNS.

Detections (%)	SNR	SNR+PNS	CBT	CBT+PNS
Lost	9	5.3	5.2	5.2
Same	91	94.7	94.8	94.8
Additional	0.2	1.7	1.9	2
Total	91.2	96.4	96.7	96.8
Recovered signals with SNR < 7 dB	1.8	27	27.6	27.3

Table 10. Comparison statistics with respect to the SNR censoring with the original noise power.

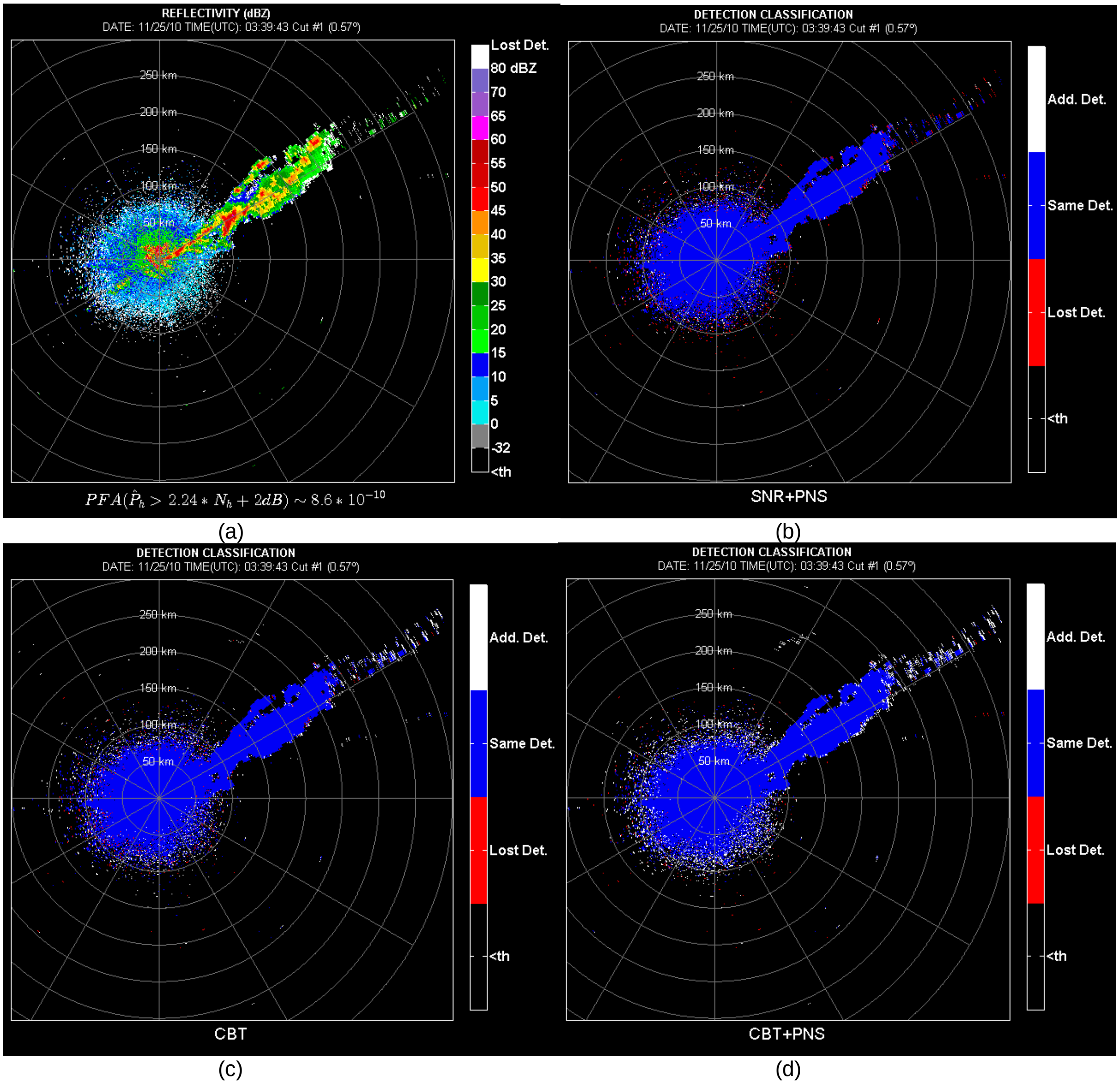

Figure 27. a) Reflectivity field (M = 28) obtained after artificially increasing the noise power and setting the SNR threshold to 2 dB with respect to the increased noise power. The lost detections are highlighted in white. Classification of detections for (b) SNR+PNS, (c) CBT, and (d) CBT+PNS.

Detections (%)	SNR	SNR+PNS	CBT	CBT+PNS
Lost	10.2	2.6	1.5	0.7
Same	89.8	97.4	98.5	99.3
Additional	0.6	1.85	4	7.2
Total	90.4	99.25	102.5	106.5
Recovered signals with SNR < 5.5 dB	11.15	75.5	86	93.3

Table 11. Comparison statistics with respect to the SNR censoring with the original noise power.

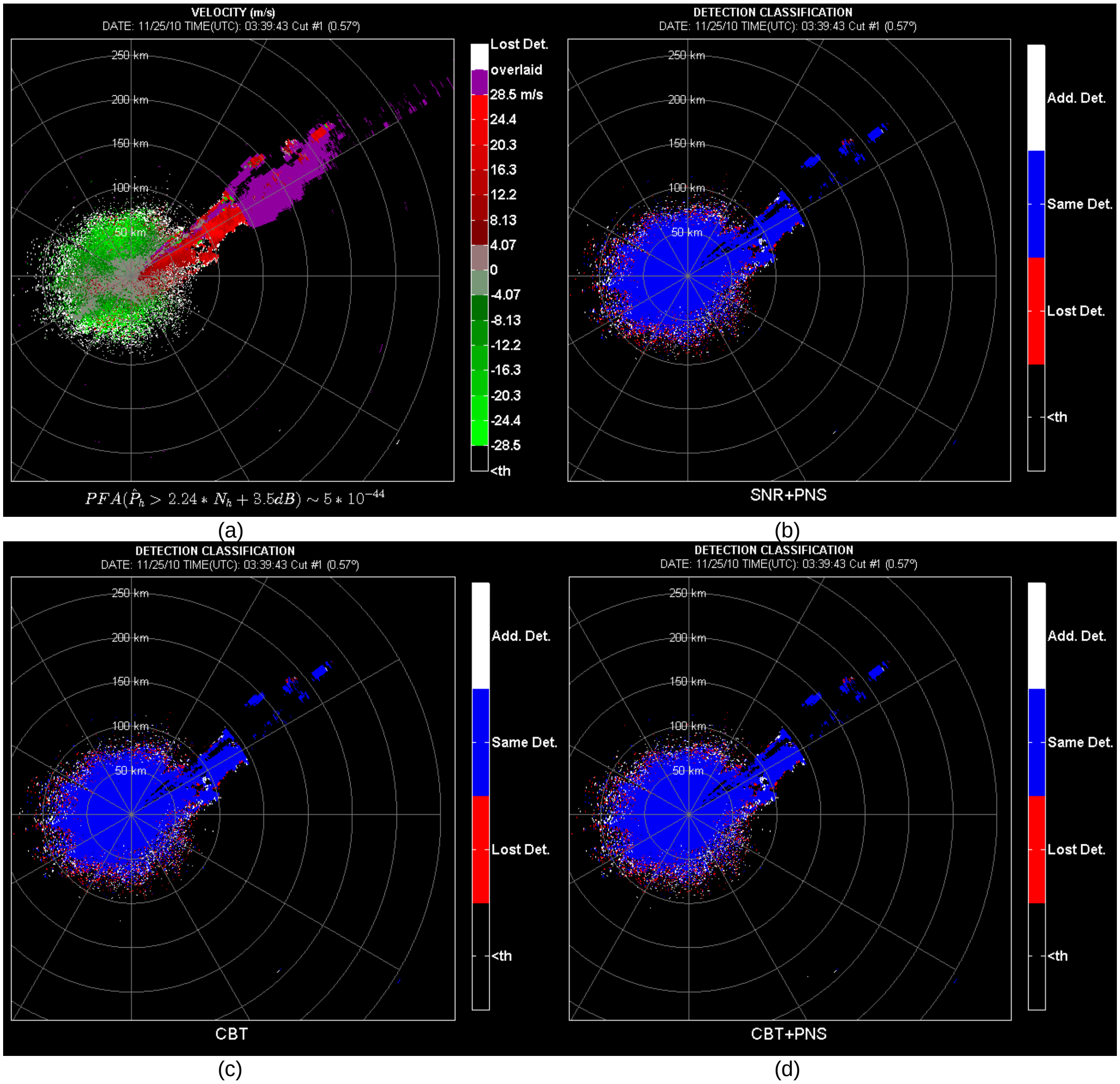

Figure 28. (a) Velocity field (*M* = 28&90) obtained after artificially increasing the noise power and setting the SNR threshold to 2 dB with respect to the increased noise power. The lost detections are highlighted in white. Detection classification for (b) SNR+PNS, (c) CBT, and (d) CBT+PNS.

Detections (%)	SNR	SNR+PNS	CBT	CBT+PNS
Lost	10.2	5.2	5.1	5.2
Same	89.8	94.8	94.9	94.8
Additional	0	3.8	3.7	4.3
Total	89.8	98.6	98.6	99.1
Recovered signals with SNR < 7 dB	1.2	25.2	25.36	25.34

Table 12. Comparison statistics with respect to the SNR censoring the with original noise power.

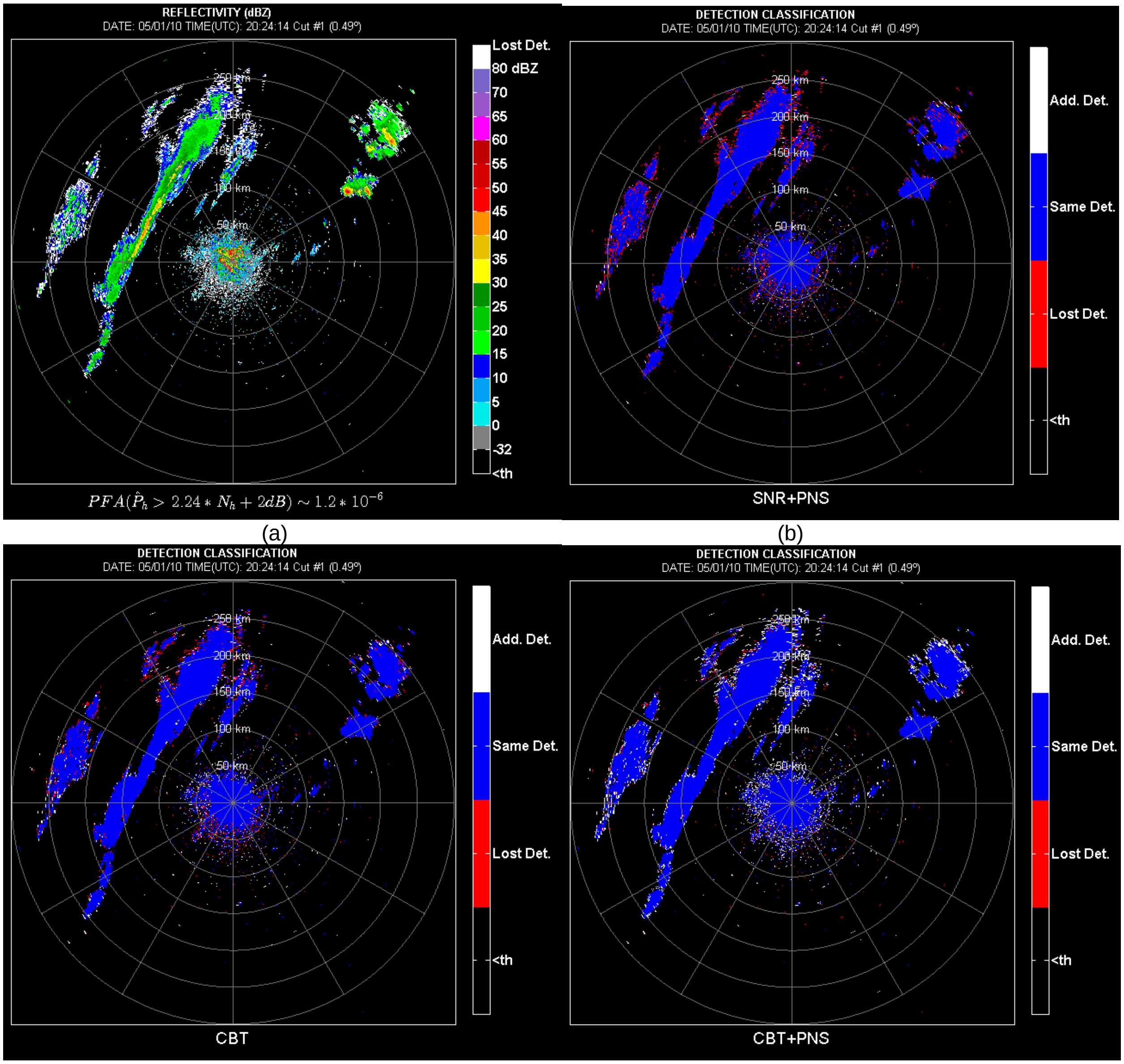

Figure 29. (a) Reflectivity field (M = 17) obtained after artificially doubling the noise power and setting the SNR threshold to 2 dB with respect to the increased noise power. The lost detections are highlighted in white. Classification of detections for (b) SNR+PNS, (c) CBT, and (d) CBT+PNS.

Detections (%)	SNR	SNR+PNS	CBT	CBT+PNS
Lost	18.2	9.8	5.8	2.5
Same	81.8	90.2	94.2	97.5
Additional	0.8	1.7	4.2	9.7
Total	82.6	91.9	98.4	107.2
Recovered signals with SNR < 5.5 dB	12.8	48.9	70	86.8

Table 13. Comparison statistics with respect to the SNR censoring with the original noise power.

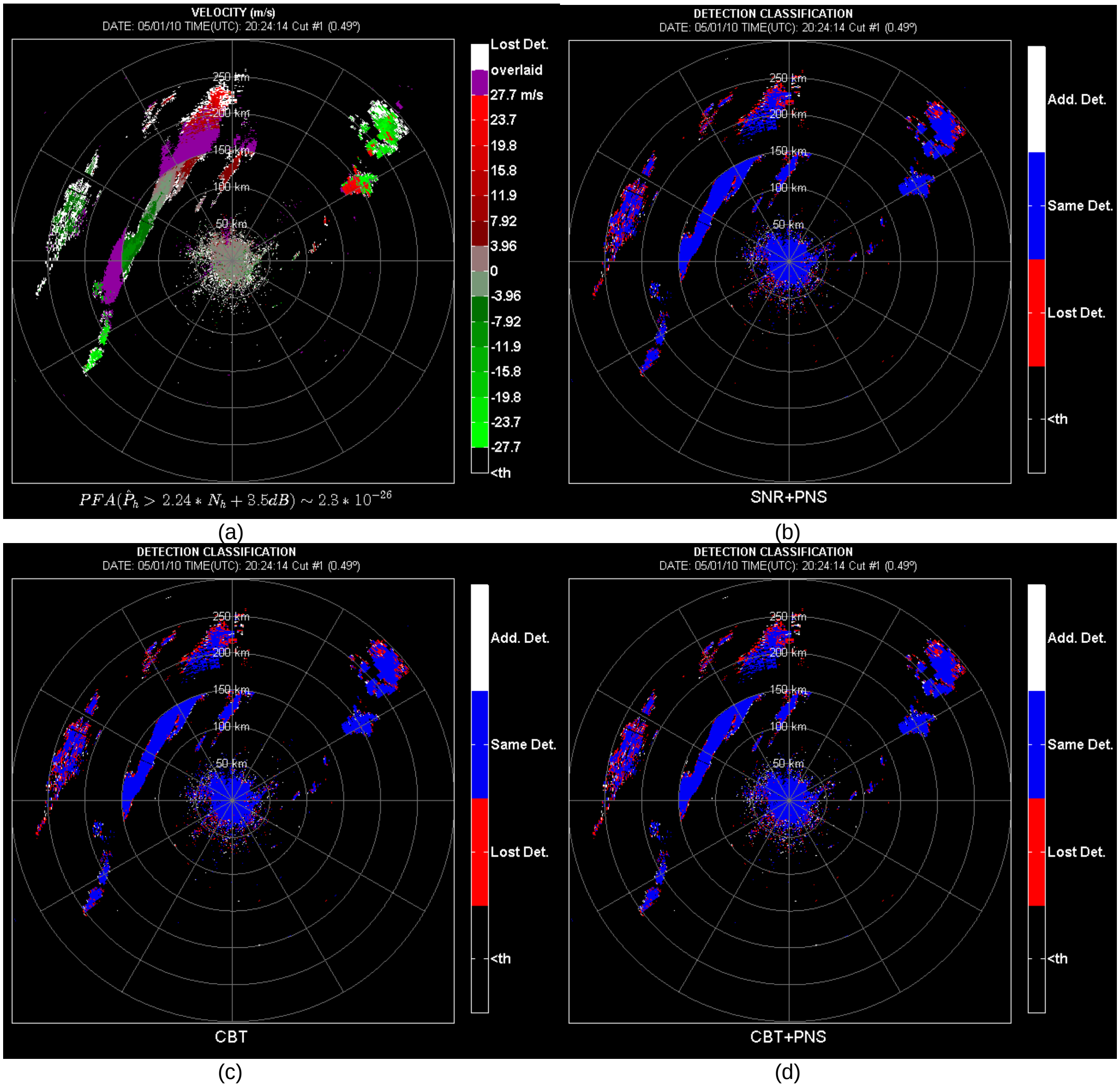

Figure 30. (a) Velocity field (M = 17&52) obtained after artificially increasing the noise power and setting the SNR threshold to 2 dB with respect to the increased noise power. The lost detections are highlighted in white. Detection classification for (b) SNR+PNS, (c) CBT, and (d) CBT+PNS.

Detections (%)	SNR	SNR+PNS	CBT	CBT+PNS
Lost	16.3	9.15	9	9
Same	83.7	90.85	91	91
Additional	0.15	3.2	3.85	4.4
Total	83.85	94.05	94.85	95.4
Recovered signals with SNR < 7 dB	1.5	25.16	25.7	25.55

Table 14. Comparison statistics with respect to the SNR censoring with the original noise power.

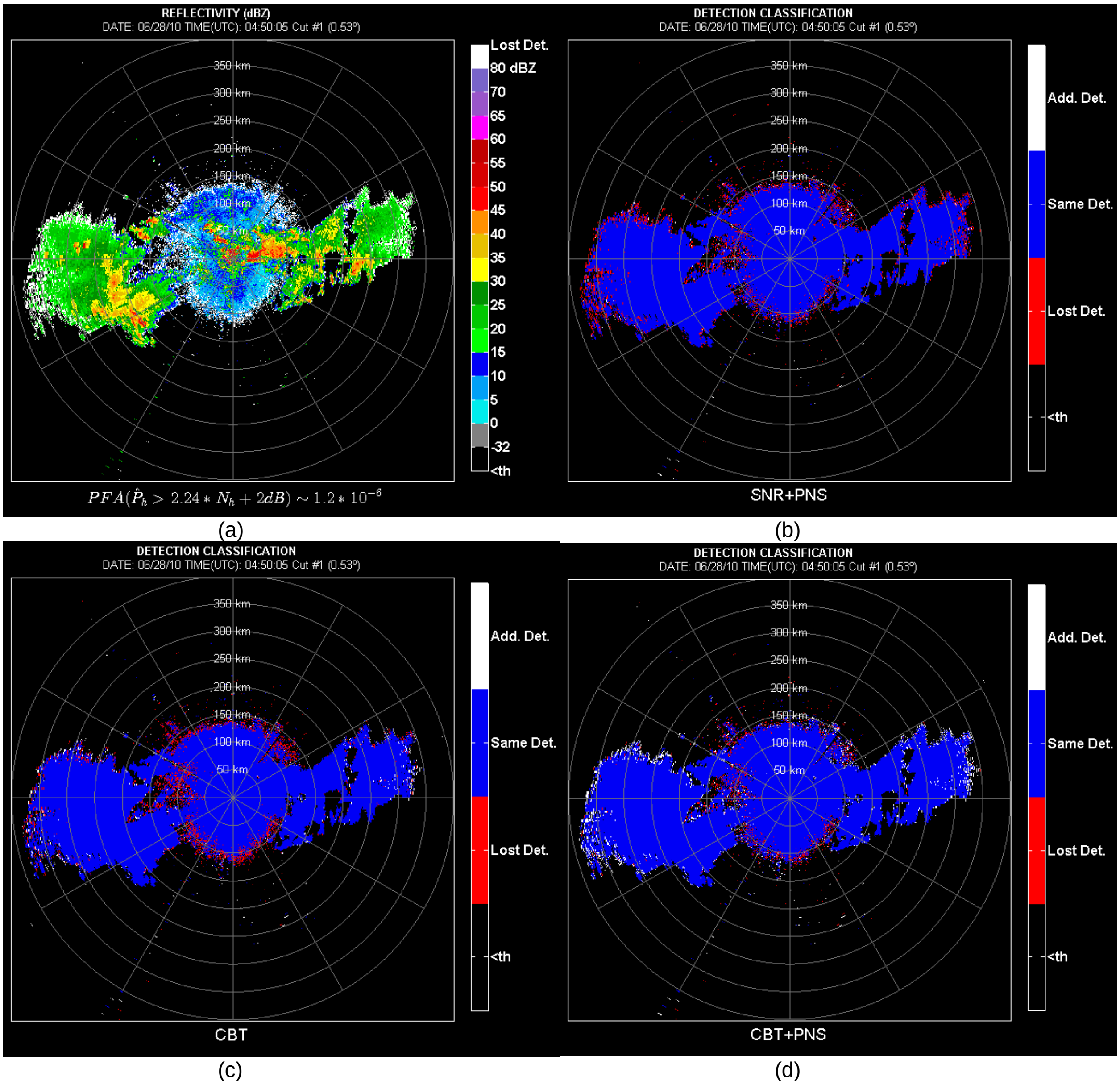

Figure 31. (a) Reflectivity field (*M* = 17) obtained after artificially increasing the noise power and setting the SNR threshold to 2 dB with respect to the increased noise power. Lost detections are highlighted in white. Classification of detections for (b) SNR+PNS, (c) CBT, and (d) CBT+PNS.

Detections (%)	SNR	SNR+PNS	CBT	CBT+PNS
Lost	10.6	5.2	5.33	2.8
Same	89.4	94.8	94.67	97.2
Additional	0.07	0.43	0.78	2.2
Total	89.47	95.23	95.45	99.4
Recovered signals with SNR < 5.5 dB	13.8	53.1	53.5	75.5

Table 15. Comparison statistics with respect to the SNR censoring with the original noise power.

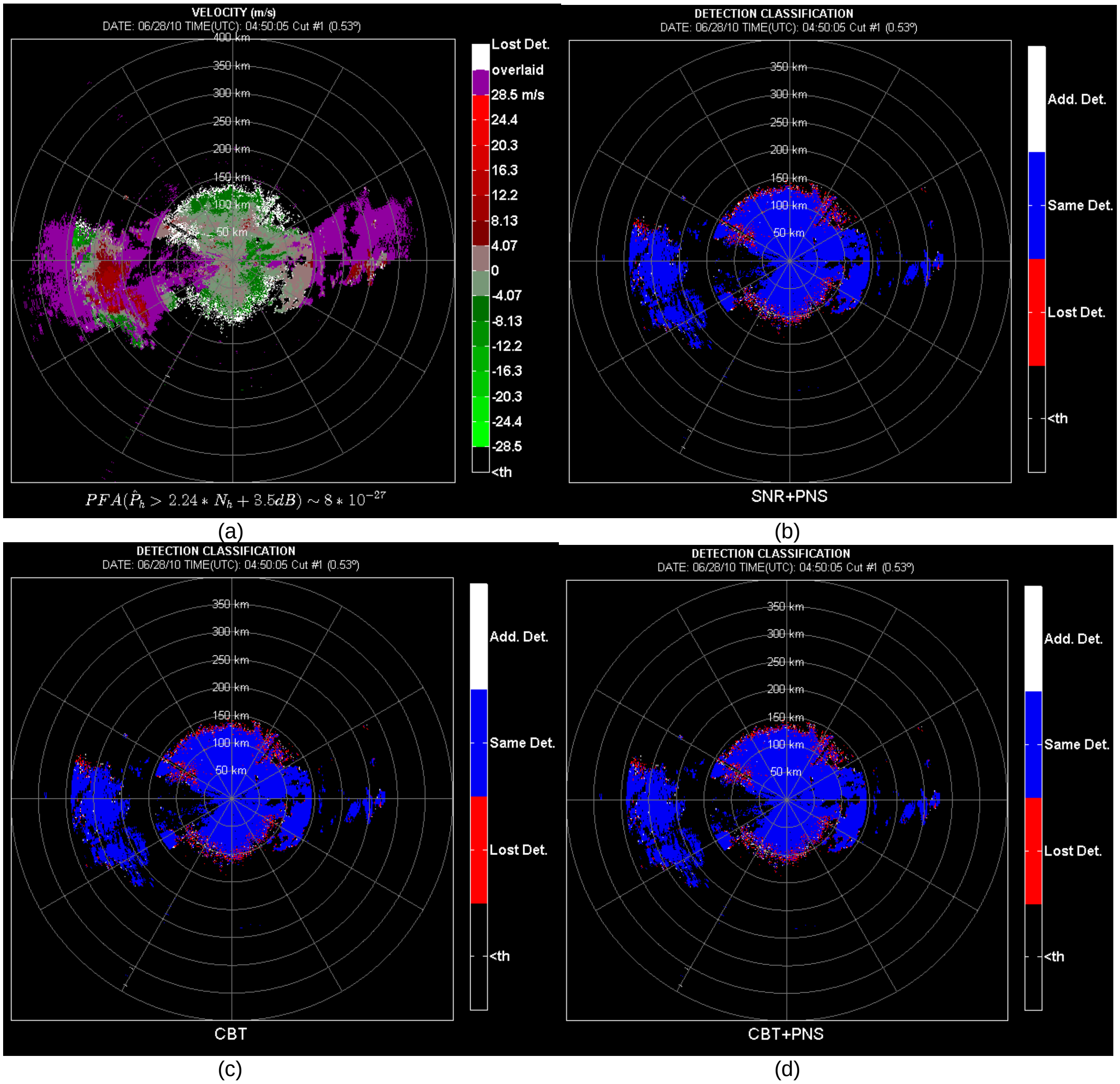

Figure 32. (a) Velocity field (M = 17&53) obtained after artificially increasing the noise power and setting the SNR threshold to 2 dB with respect to the increased noise power. The lost detections are highlighted in white. Detection classification for (b) SNR+PNS, (c) CBT, and (d) CBT+PNS.

Detections (%)	SNR	SNR+PNS	CBT	CBT+PNS
Lost	9	5	5	5
Same	91	95	95	95
Additional	0.2	1	0.8	1
Total	91.2	96	95.8	96
Recovered signals with SNR < 7 dB	3.2	36.4	36.14	36.12

Table 16. Comparison statistics with respect to the SNR censoring with the original noise power.

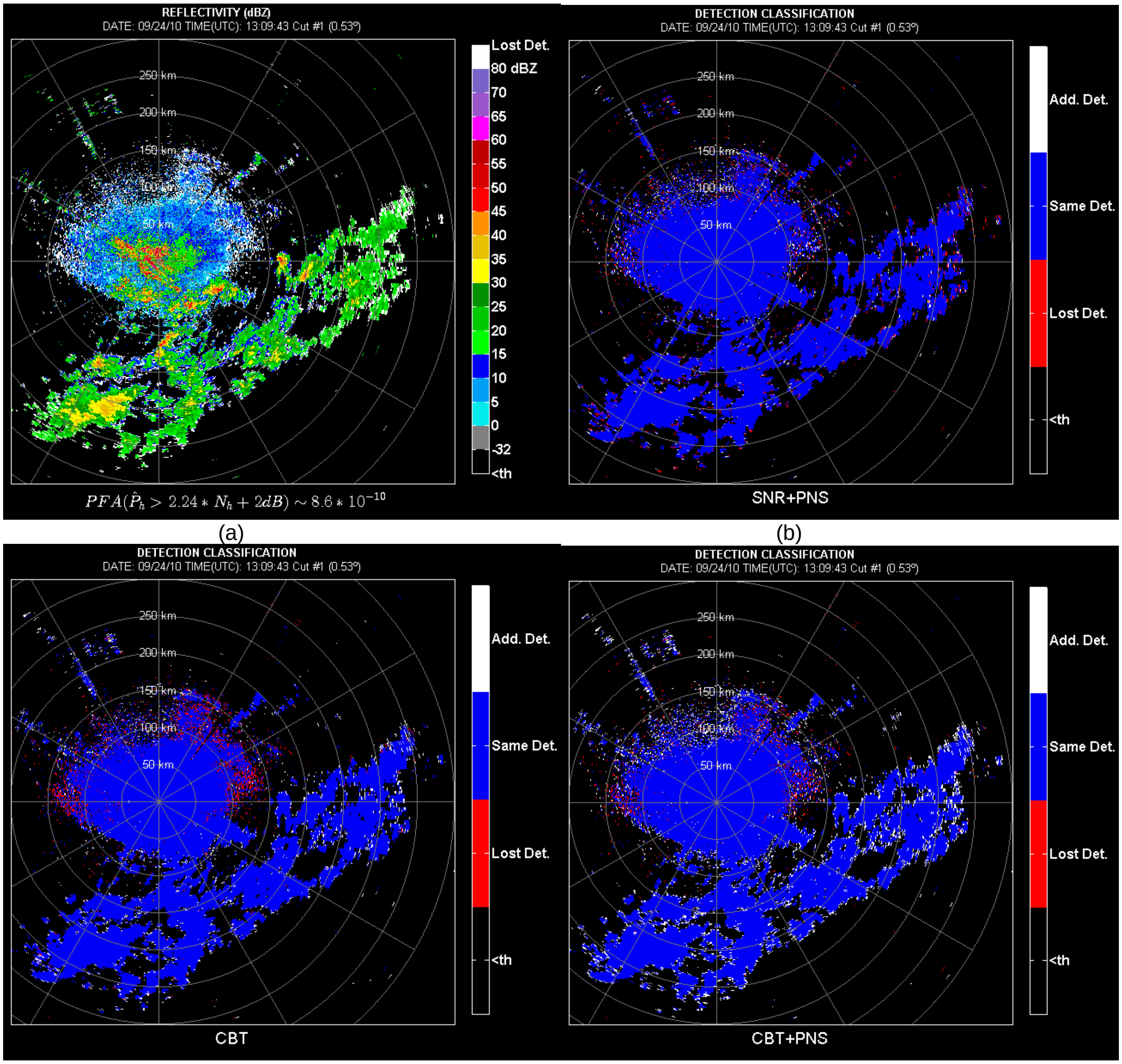

(c) (d)

Figure 33. (a) Reflectivity field (*M* = 28) obtained after artificially increasing the noise power and setting the SNR threshold to 2 dB with respect to the increased noise power. Lost detections are highlighted in white. Classification of detections for (b) SNR+PNS, (c) CBT, and (d) CBT+PNS.

Detections (%)	SNR	SNR+PNS	CBT	CBT+PNS
Lost	11.7	2.67	3.4	1.9
Same	88.3	97.33	96.6	98.1
Additional	0.2	1.6	2.4	5.3
Total	88.5	98.93	99	103.4
Recovered signals with SNR < 5.5 dB	10.31	77.84	72.15	84.7

Table 17. Comparison statistics with respect to the SNR censoring with the original noise power.

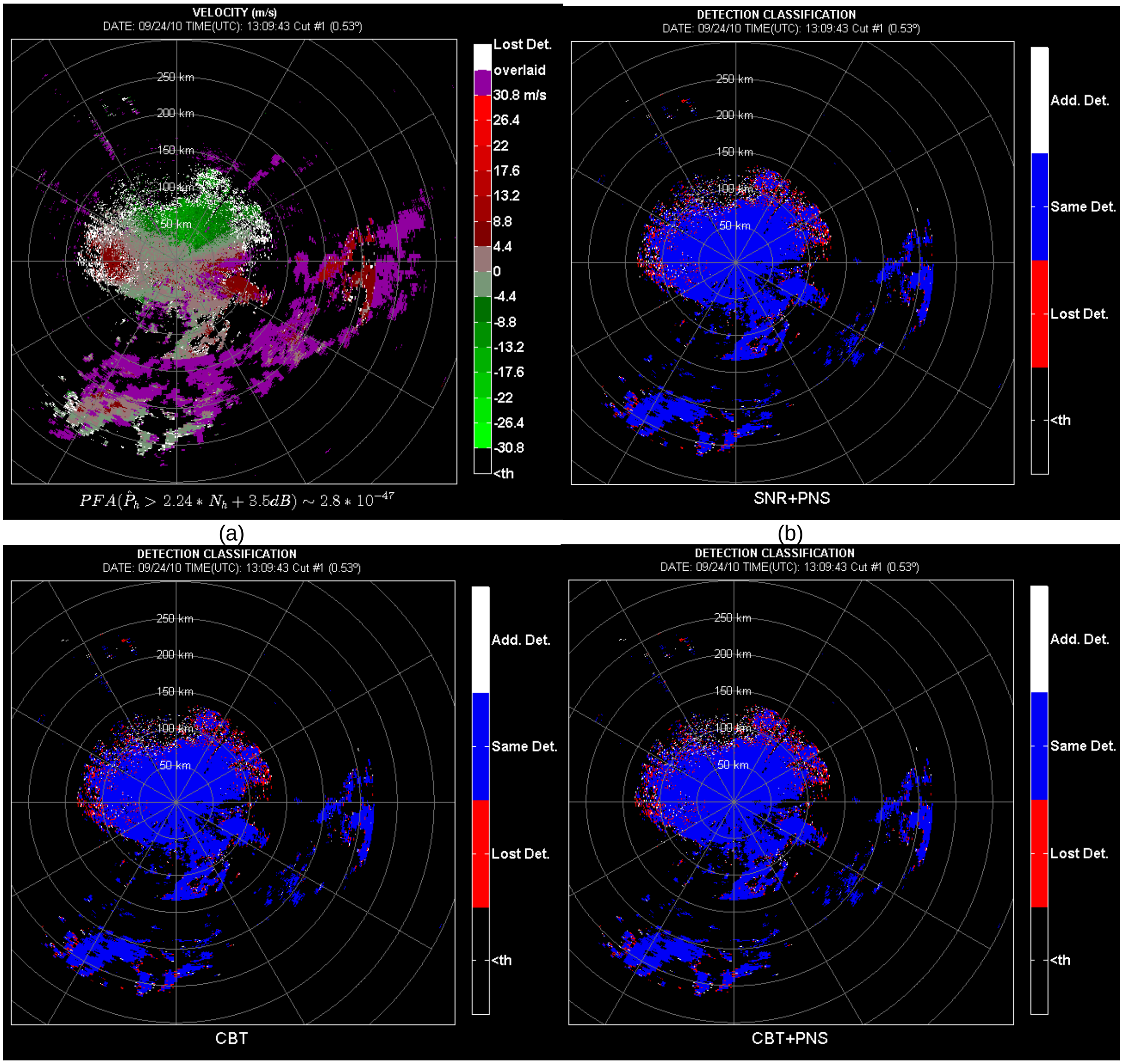

(c) (d)

Figure 34. (a) Velocity field (*M* = 28&97) obtained after artificially increasing the noise power and setting the SNR threshold to 2 dB with respect to the increased noise power. The lost detections are highlighted in white. Detection classification for (b) SNR+PNS, (c) CBT, and (d) CBT+PNS.

Detections (%)	SNR	SNR+PNS	CBT	CBT+PNS
Lost	9.7	5	5.1	5.1
Same	90.3	95	94.9	94.9
Additional	0.17	2.2	1.8	2.1
Total	90.47	97.2	96.7	97
Recovered signals with SNR < 7 dB	1.9	35.65	35	35

Table 18. Comparison statistics with respect to the SNR censoring with the original noise power.

Detections (%)	SNR	SNR+PNS	CBT	CBT+PNS
Lost	12.98	5.594	4.066	1.98
Same	87.02	94.406	95.934	98.02
Additional	0.454	1.356	2.916	6.32
Total	87.474	95.762	98.85	104.34
Recovered signals with SNR < 5.5 dB	12.112	60.668	70.53	85.38

(a)

Detections (%)	SNR	SNR+PNS	CBT	CBT+PNS
Lost	10.84	5.93	5.88	5.9
Same	89.16	94.07	94.12	94.1
Additional	0.144	2.38	2.41	2.76
Total	89.304	96.45	96.53	96.86
Recovered signals with SNR < 7 dB	1.88	29.832	29.92	29.802

(b)

Table 19. Average comparison statistics with respect to the SNR censoring with original noise power for (a) surveillance and (b) split scans.

6. SUMMARY

Methods to threshold polarimetric weather radar data were investigated and compared. Motivation comes from the SNR loss in radars that transmit (and receive) simultaneously electromagnetic waves at horizontal and vertical polarizations. The forthcoming dual polarization upgrade of the WSR-88D network will employ this technique resulting in a 3.5 dB SNR drop. It has been shown that this will lead to a noticeable decrease in detection of weather features (i.e., coverage), if current censoring scheme is retained. Thus, it is desirable to mitigate the effects of this loss in sensitivity. So far, two approaches to increase WSR-88D radar sensitivity have been proposed. One operates on time-series from horizontal and vertical channel at each range position. It combines time-series in such manner that utilizes coherencies along sample-time and between channels to improve detection. As opposed to this technique, other operates in two dimensions and is based on supposition that the likelihood of adjacent detections is much less in a noise only case and increases significantly with the presence of signals. Clearly, the second technique requires a two dimensional map of detections to operate on. Such map can be created by any censoring technique that operates on time-series, at each range position. Consequently, this "spatial" technique was combined with the SNR based (i.e., legacy) censoring, and with the coherency based one. Both combinations were vetted through simulations and experimentally on time-series. The analysis shows that the combination of the coherency and spatial censoring produces the best results. Moreover, simulations show that, when combined, these two techniques have the potential to not only fully regain the lost weather features, but even increase coverage; with respect to the single-polarization system using the "legacy" SNR based censoring.

ACKNOWLEDGEMENT

Funding for part of this research was provided by NOAA/Office of Oceanic and Atmospheric Research under NOAA-University of Oklahoma Cooperative Agreement #NA17RJ1227, U.S. Department of Commerce. The statements, findings, conclusions, and recommendations are those of the author(s) and do not necessarily reflect the views of NOAA or the U.S. Department of Commerce. In addition, we would like to thank the Radar operations Center (ROC) for providing time-series used in this research.

REFERENCES

Doviak, R.J., and D.S. Zrnić, 1993: *Doppler radar and weather observations*. Academic Press, 562 pp.

Fang M., R. J. Doviak, and V. Melnikov, 2003: Spectrum Width Measured by WSR-88D: Error Sources and Statistics of Various Weather Phenomena, *J. Atmos.Oceanic Technol.*, **21**, 888-904.

Ice L. R., D. S. Saxion, O. E. Boydstun, W. D. Zittel, R. W. Hall, G. S. Cate, A. D. Free, R. D. Rhoton, R. W. Macemon, and B. Walker, 2011: Sensitivity of Operational Weather Radars, *27th Conference on Interactive Information Processing Systems (IIPS)*, Seattle, VA.

Ivić I. R., D.S. Zrnić., and T. -Y. Yu, 2009: Use of Coherency to Improve Signal Detection in Dual-

Polarization Weather Radars, *J. Atmos.Oceanic Technol*., **26**, 2474–2487.

Ivić I. R., and S. M. Torres, 2011: Online Determination of Noise Level in Weather Radars*, 27th Conference on Interactive Information Processing Systems (IIPS)*, Seattle, VA***.***

Melnikov V. M., and P. T. Schlatter, 2011: Enhancing Sensitivity on the Polarimetric WSR-88D, *27th Conference on Interactive Information Processing Systems (IIPS)*, Seattle, VA*.*

Scharfenberg K. A., K. L. Elmore, E. Forren, V. Melnikov, and D. S. Zrnić, 2005: Estimating the impact of a 3-dB sensitivity loss on WSR-88D data, *32nd Conference on Radar Meteorology*.

SIGMET, 2008: Chapter 5. *RVP8 User's Manual*, 63 pp.

Zrnić D.S., 1975: Simulation of weather like Doppler spectra and signals, *J. Appl. Meteorol*., 619-620.